*J. Fluid Mech.* (1988), *vol.* 194, *pp.* 45–77
*Printed in Great Britain*



# Impulsively started flow around a circular cylinder by the vortex method

By P. A. SMITH AND P. K. STANSBY
Simon Engineering Laboratories, University of Manchester, M13 9PL, UK

(Received 26 January 1987 and in revised form 15 January 1988)

Impulsively started, viscous, incompressible flows around a circular cylinder are simulated by a Lagrangian vortex solution of the vorticity equation using random walks for diffusion and the vortex-in-cell method for convection in a fractional-step scheme. Vortices are introduced around the surface at each timestep to satisfy the zero-slip condition. In the range of Reynolds numbers $2.5 \times 10^2$ to $10^5$, comparisons with two analytical solutions, valid for small times ($t < 1$), show reasonable agreement. For somewhat longer times ($t < 5$), for a similar range of Reynolds numbers, comparisons are made with accurate Eulerian numerical solutions and with careful flow-visualization experiments. Agreement is good provided a sufficiently large number of vortices is introduced per timestep. The number required increases as Reynolds number increases. If too few are introduced, the vorticity in the wake tends to roll up too tightly. The vortex method remains stable, whereas Eulerian schemes have been reported to become eventually unstable unless upwind differencing is used, reducing accuracy.

## 1. Introduction

The use of the fractional-step, Lagrangian vortex scheme originally proposed by Chorin (1973, 1978) to solve the vorticity equation in two dimensions is the subject of considerable research effort (e.g. Leonard 1980; Chorin 1980; Roberts 1985). The method has shown potential for the simulation of flows around cylindrical bodies (e.g. Cheer 1983; Stansby & Dixon 1983; Smith & Stansby 1987). The vorticity field is discretized into a set of particles (vortices). In the time-stepping procedure, vortices are created on the cylinder surface to satisfy the zero-slip condition, random walks are imposed to simulate the process of viscous diffusion and vortices are finally convected in an inviscid calculation. A large number of vortices is required in order to achieve a good flow representation and these are handled efficiently using the vortex-in-cell method of velocity calculation. We use a single, radially expanding polar mesh, coincident with the surface of the cylinder along its inner boundary, enabling the surface boundary conditions to be satisfied simply and precisely. The operation count for each timestep is of order $N \log N$, where $N$ is the number of grid points on the mesh, whereas direct summation for $L$ vortices would produce an operation count of order $L^2$. The use of the vortex-in-cell method is thus advantageous in terms of efficiency and precision of the boundary conditions at the cylinder surface.

Impulsively started flow around a circular cylinder has been the subject of much study for fundamental and practical reasons. It is well known from experiment (Tritton 1977) that flows of long duration become three-dimensional when the Reynolds number is increased above about 100. The initial stages are, however,

thought to be almost two-dimensional and careful flow visualization experiments (Bouard & Coutanceau 1980) provide valuable data for comparison with numerical solutions. At early times the flow undergoes gross changes, with moving separation positions, the formation of recirculating regions and the formation of secondary eddies. These phenomena are dependent on Reynolds number, presenting a severe test for any prediction method.

For very small times ($t < 1$, non-dimensionalized using the cylinder radius and the onset flow velocity) we compare with two analytical solutions based on time-series expansions (Collins & Dennis 1973*a*; Bar-Lev & Yang 1975). For longer times ($t < 5$) we compare with the Eulerian finite-difference solutions of Collins & Dennis (1973*b*) and Ta Phuoc Loc & Bouard (1985). The latter show that their computed results, including importantly some velocities in the near wake, are in close agreement with the experiments of Bouard & Coutanceau (1980), providing an ideal check for our vortex method. In this paper we present a comprehensive description of the flow, including the time variation of surface pressure and surface vorticity distributions, separation positions, forces, streamline patterns and some velocities in the near wake.

The accurate Eulerian formulations mentioned above do not include upwind differencing, without which such schemes have been reported to become eventually unstable (e.g. Telionis 1981; Davis & Moore 1982). Collins & Dennis (1973*b*) specifically mention the breakdown of their integration procedure at a time which decreases with increasing Reynolds number. The use of upwind differencing reduces accuracy. The vortex method, on the other hand, remains stable and it is desirable to show that this alternative method, which is relatively easy to set up, can predict accurately the detailed, highly transient flow structures which occur during the starting flow around a cylinder.

## 2. Theory

The viscous flow of an incompressible fluid with constant kinematic viscosity ($\nu$) and density ($\rho$) past a circular cylinder is governed by the Navier–Stokes and the continuity equations. In non-dimensional form, these may be written

$$\frac{\partial \boldsymbol{u}}{\partial t} = -\tfrac{1}{2}\nabla P - (\boldsymbol{u}\cdot\nabla)\,\boldsymbol{u} + 2Re^{-1}\nabla^2\boldsymbol{u}, \tag{1}$$

$$\nabla\cdot\boldsymbol{u} = 0. \tag{2}$$

The dependent variables are the velocity ($\boldsymbol{u}$) and pressure ($P$). The cylinder radius ($a$) and the speed of the distant flow ($U$) are respectively the reference length and velocity. $Re = 2Ua/\nu$ is the Reynolds number. The dimensional velocity ($\boldsymbol{u}^*$), time ($t^*$) and pressure ($P^*$) are given by

$$\boldsymbol{u}^* = U\boldsymbol{u}, \quad t^* = at/U, \quad P^* = \tfrac{1}{2}\rho U^2 P. \tag{3}$$

In order to simulate a flow numerically by the vortex method, (1) and (2) are recast as a Poisson equation for the stream function, $\psi$,

$$\nabla^2\psi = -\omega, \tag{4}$$

and a transport equation for the component of vorticity normal to the two-dimensional plane of the flow, $\omega$,

$$\frac{\partial \omega}{\partial t} = -(\boldsymbol{u}\cdot\nabla)\,\omega + 2Re^{-1}\nabla^2\omega, \tag{5}$$

$\omega$ is related to $\boldsymbol{u}$ through the equation

$$\omega = |\nabla \wedge \boldsymbol{u}|. \tag{6}$$

The motion is referred to a polar coordinate system $(r, \theta)$. The cylinder surface is at $r = 1$ and $(1, 0)$ coincides with the upstream stagnation point of the potential flow. If $t = 0$ defines the start of the motion, the boundary conditions for the solution of (4) are that, for $t > 0$

$$\psi = 0 \quad \text{when } r \leqslant 1, \tag{7a}$$

$$\frac{\partial \psi}{\partial r} \to -\sin\theta \quad \text{as } r \to \infty. \tag{7b}$$

Those for (5) are that, for $t > 0$

$$\boldsymbol{u} \cdot \hat{\boldsymbol{\theta}} = 0 \quad \text{when } r \leqslant 1, \tag{8a}$$

$$\omega \to 0 \quad \text{as } r \to \infty. \tag{8b}$$

The boundary conditions set the velocity within the cylinder surface to zero (equations (7*a*) and (8*a*)) and state that the vorticity and the perturbation it causes in the flow at large distance from the cylinder are small (equations (7*b*) and (8*b*)).

$\boldsymbol{u}$ is related to $\psi$ through the equation

$$\boldsymbol{u} = \frac{\hat{\boldsymbol{r}}}{r}\frac{\partial \psi}{\partial \theta} - \hat{\boldsymbol{\theta}}\frac{\partial \psi}{\partial r}, \tag{9}$$

where $\hat{\boldsymbol{r}}$ and $\hat{\boldsymbol{\theta}}$ are unit vectors.

## 3. Method

The distribution of vorticity is approximated by a set of $L$ discrete point vortices, such that

$$\omega = \sum_{i=1}^{L} \Gamma_i \delta[\boldsymbol{r} - \boldsymbol{r}_i], \tag{10}$$

where $\Gamma_i$ and $\boldsymbol{r}_i$ are respectively the circulation and position of the $i$th vortex and $\delta[\boldsymbol{r}]$ is the Dirac delta function. The distribution is advanced through successive time steps ($\Delta t$) by the method summarized below.

(i) Poisson's equation for the stream function is solved on the vortex-in-cell mesh, and the solution is used to create a set of new point vortices on the cylinder surface, which satisfy the zero-slip condition.

(ii) Viscous diffusion is simulated by adding a random walk to the positions of the discrete vortices. Vortices crossing the surface are reflected back into the flow.

(iii) The velocity of each vortex is calculated by the vortex-in-cell method and their positions are advanced to give a first-order prediction.

(iv) New velocities are calculated, again using the vortex-in-cell method, to give a second-order correction to the vortex positions.

The components of the method are now described in detail.

### 3.1. *The solution of Poisson's equation*

A modified polar coordinate system $(r', \theta)$ is introduced. Equation (4) may then be written

$$\frac{\partial^2 \psi}{\partial \theta^2} + a(r')\frac{\partial^2 \psi}{\partial r'^2} + b(r')\frac{\partial \psi}{\partial r'} = -\omega r^2, \tag{11a}$$

where
$$a(r') = \left(r\frac{\mathrm{d}r'}{\mathrm{d}r}\right)^2, \tag{11b}$$

$$b(r') = r\frac{\mathrm{d}r'}{\mathrm{d}r} + r^2\frac{\mathrm{d}^2r'}{\mathrm{d}r^2}, \tag{11c}$$

$$r = B(\mathrm{e}^{Ar'} - 1) + 1. \tag{11d}$$

Equation (11) may be solved using a fast Fourier transform technique, since only the Poisson operator includes the coordinate $\theta$; the technique is advantageous because of its low operation count (Hockney 1970). A $129 \times 200$ polar mesh was used, with a uniform mesh size in the coordinate system $(r', \theta)$, defined over an annular region outside the cylinder surface ($1 < \mathrm{r} < r_0$). At the node $(i,j)$, $r' = j$ and $\theta = i\Delta\theta$ ($\Delta\theta = 2\pi/128$; $i = 0, \ldots, 128$; $j = 0, \ldots, 199$). Fine resolution is required near to the surface of the cylinder, whereas progressively coarser resolution is acceptable with increasing radial distance. The constants $A$ and $B$ in equation (11*d*) are fixed by the radial mesh spacing at the cylinder surface (a spacing equal to the standard deviation of the random walk was found to be suitable in the following computations) and by the value of the outer radius ($r_0$). $r_0$ must be sufficiently large for (7*b*) to be an adequate approximation and for all the vortices to be contained within the mesh (equation (8*b*)). Results are presented in §5, for times up to $t = 0.8$, which show insensitivity to the choice of $r_0$ in the range 5 to 100.

The circulation carried by each vortex is distributed between the four corner nodes of the cell in which the vortex is contained. An area-weighting scheme is used (Christiansen 1973). If $\Gamma(i,j)$ is the total circulation associated with the node $(i,j)$, the nodal value of $\omega$ is given by
$$\omega(i,j) = \frac{\Gamma(i,j)}{r\Delta\theta}\frac{\mathrm{d}r'}{\mathrm{d}r}\bigg|_{r'=j}. \tag{12}$$

Both $-\omega r^2$ and $\psi$ are expanded as Fourier series in $\theta$ and substituted into the finite-difference analogue of (11*a*), yielding a set of tridiagonal simultaneous equations for each harmonic amplitude of $\psi$, which are solved by Gauss elimination.

### 3.2. *Creation of vorticity*

New vortices are created along $r = 1$ at each time increment, modelling the creation of vorticity due to the action of viscosity at a solid boundary. The vortices are assigned circulations which modify the source term in (11*a*), so that the boundary condition on the tangential component of velocity (equation (8*a*)) is satisfied. Since $\psi \neq \psi(r)$ along $r = 1$ (equation (7*a*)), the finite difference analogue of (11*a*) reduces to
$$\omega(i,0) = -a(0)[\psi(i,1) - 2\psi(i,0) + \psi(i,-1)] - \tfrac{1}{2}b(0)[\psi(i,1) - \psi(i,-1)]. \tag{13}$$

In order to satisfy the boundary conditions (equations (7*a*) and (8*a*)) the stream function must be a constant at all points inside the cylinder. We therefore set $\psi(i,-1) = \psi(i,0) = 0$. Equation (13) then becomes
$$\omega(i,0) = -[a(0) + \tfrac{1}{2}b(0)]\psi(i,1). \tag{14}$$

From (12), an additional circulation $\Gamma(i,0)$ must be introduced at the surface node $(i,0)$, given by
$$\Gamma(i,0) = \Delta\theta\omega(i,0)\frac{\mathrm{d}r}{\mathrm{d}r'}\bigg|_{r'=0} - \Gamma'(i,0), \tag{15}$$

where $\Gamma'(i,0)$ is the circulation distributed onto the mesh from the old vortices. The

additional circulation $\Gamma(i,0)$ is shared between the newly created vortices. The number of new vortices created at each surface node ($n_v$) was determined by numerical experiment (§5).

### 3.3. *Time marching*

Following the method of Chorin (1973, 1978), (5) is split into a linear diffusion equation

$$\left[\frac{\partial\omega}{\partial t}\right]_1 = 2Re^{-1}\nabla^2\omega, \tag{16}$$

and the nonlinear Euler equation

$$\left[\frac{\partial\omega}{\partial t}\right]_2 = -(\boldsymbol{u}\cdot\boldsymbol{\nabla})\,\omega. \tag{17}$$

The processes of viscous diffusion and of convection, denoted by the suffices 1 and 2 respectively, are considered separately. At each timestep, (16) and (17) are solved consecutively, in order to approximate the solution of the complete vorticity equation.

Equation (16) is solved by adding a random walk to the positions of the vortices, based on a normal distribution with zero mean and variance $2\nu\Delta t$ (Wax 1954). If $g$ and $h$ are two numbers selected from the normal distribution and $(x_1, y_1)$ and $(x_2, y_2)$ are respectively the Cartesian coordinates of a vortex before and after displacement, then

$$x_2 = x_1 + g, \quad y_2 = y_1 + h, \tag{18}$$

$g$ and $h$ are reselected for each vortex and at each timestep. Following the random walk, if a vortex lies inside the cylinder, it is reflected to its exterior mirror-image position (Chorin 1978).

It may be shown that equation (17) is solved by convecting the vortices in the velocity field, while each vortex preserves its circulation (Batchelor 1981). The velocity of a vortex is obtained from the finite difference analogue of (9), using the nodal values of $\psi$ associated with the cell containing the vortex. The convective displacements are calculated using a second-order Runge–Kutta method. If $\boldsymbol{u} = \boldsymbol{u}(\boldsymbol{r}, t)$ is the velocity of a vortex, and $\boldsymbol{r}_1$ and $\boldsymbol{r}_2$ are respectively its positions before and after displacement

$$\boldsymbol{r}_2 = \boldsymbol{r}_1 + \tfrac{1}{2}(\boldsymbol{d}_1 + \boldsymbol{d}_2), \tag{19a}$$

where

$$\boldsymbol{d}_1 = \boldsymbol{u}(\boldsymbol{r}_1, t)\,\Delta t, \tag{19b}$$

$$\boldsymbol{d}_2 = \boldsymbol{u}(\boldsymbol{r}_1 + \boldsymbol{d}_1, t + \Delta t)\,\Delta t. \tag{19c}$$

Second-order accuracy is obtained at the expense of a second solution of the Poisson equation, which is required for the calculation of $\boldsymbol{d}_2$.

Beale & Majda (1981) showed that the viscous-splitting algorithm used here (equations (16) and (17)) converges at a rate proportional to $Re^{-1}\Delta t$. The random-walk method gives an exact solution of (16); there is no error associated with the timestep length. At high Reynolds numbers, therefore, when $Re^{-1}\Delta t$ is small, the accuracy of the method is determined by the accuracy of the solution of (17): second order in $\Delta t$.

A timestep of 0.02 was found to be small enough for convergence in the following computations (§5).

## 4. Surface pressure, forces and vorticity

### 4.1. *Surface pressure*

The velocity and its time derivative are equal to zero along $r = 1$. Equation (1) therefore simplifies to

$$\tfrac{1}{2}\nabla P = 2Re^{-1}\nabla^2 \boldsymbol{u} = 2Re^{-1}[\nabla(\nabla \cdot \boldsymbol{u}) - \nabla \wedge \nabla \wedge \boldsymbol{u}]. \tag{20}$$

Substituting (2) and (6) into (20) and forming a scalar product with the unit vector $\hat{\boldsymbol{\theta}}$

$$\frac{1}{2}\frac{\partial P}{\partial \theta} = -2Re^{-1}\frac{\partial \omega}{\partial r}. \tag{21}$$

The right-hand side of (21) represents the flux of circulation per unit length across the cylinder surface, modelled over one time increment by the creation of circulation $\Gamma(i, 0)$ $(i = 0, \ldots, 128)$ at the surface nodes (equation (15)). $\Delta P_i$, the change in pressure along the minor arc $i - \frac{1}{2} < \theta < i + \frac{1}{2}$, is given by

$$\Delta P_i = 2\Gamma(i, 0)/\Delta t. \tag{22}$$

The pressure distribution around the surface of the cylinder is obtained by a summation of these pressure increments.

### 4.2. *Force coefficients*

The form drag and lift coefficients, corresponding to the force components directed respectively along $\theta = \pi$ and $\theta = \frac{1}{2}\pi$, can be calculated from an integration of the pressure distribution, obtained from equation (22).

$$C_{\mathrm{D}} = \frac{\Delta\theta}{\Delta t}\sum_{j=0}^{128}\left[\cos(j\,\Delta\theta)\sum_{i=1}^{j}\Gamma(i, 0)\right], \tag{23a}$$

$$C_{\mathrm{L}} = -\frac{\Delta\theta}{\Delta t}\sum_{j=0}^{128}\left[\sin(j\,\Delta\theta)\sum_{i=1}^{j}\Gamma(i, 0)\right]. \tag{23b}$$

### 4.3. *Surface vorticity*

The surface vorticity $[\omega_0(\theta)]$ cannot be taken from the nodal values of $\omega$ along $r = 1$; the area-weighting scheme smooths the vorticity distribution across the cylinder surface, so that $|\omega_0(i\,\Delta\theta)| \neq |\omega(i, 0)|$. It may, however, be obtained from the nodal values $\omega(i, 1)$. Expressing $\omega$ as a Taylor series in $r$ and, using (21), the following first-order approximation may be made

$$\omega_0(i\,\Delta\theta) \simeq \omega(i, 1) + \tfrac{1}{4}Re\frac{\partial P}{\partial \theta}\frac{\mathrm{d}r}{\mathrm{d}r'}\bigg|_{r'=0}. \tag{24}$$

Substituting (22) into (24)

$$\omega_0(i\,\Delta\theta) \simeq \omega(i, 1) + \frac{Re\,\Gamma(i, 0)}{2\,\Delta\theta\,\Delta t}\frac{\mathrm{d}r}{\mathrm{d}r'}\bigg|_{r'=0}. \tag{25}$$

## 5. Numerical parameters

Numerical experiments were carried out in order to determine suitable values for $n_{\mathrm{v}}$, $r_0$, $\Delta t$.

The impulsive start results in the creation of a large circulation at each of the surface nodes at the first timestep. $n_{\mathrm{v}}$, the number of vortices created at each of the

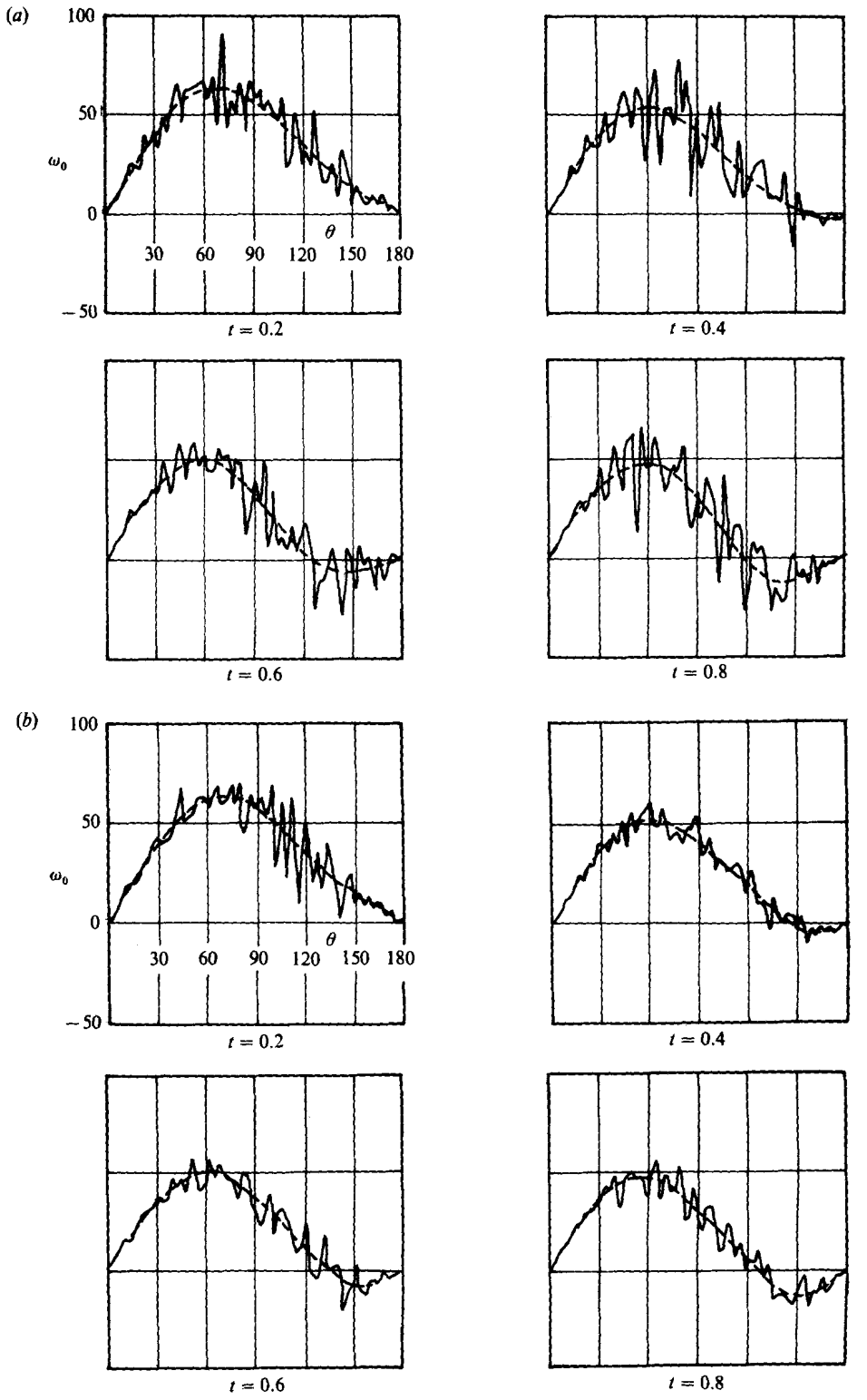


FIGURE 1. Time development of the surface vorticity distribution about a circular cylinder ($r_0 = 25$). (*a*) $n_v = 1$; (*b*) $n_v = 3$. ——, unsmoothed; – – –, smoothed.

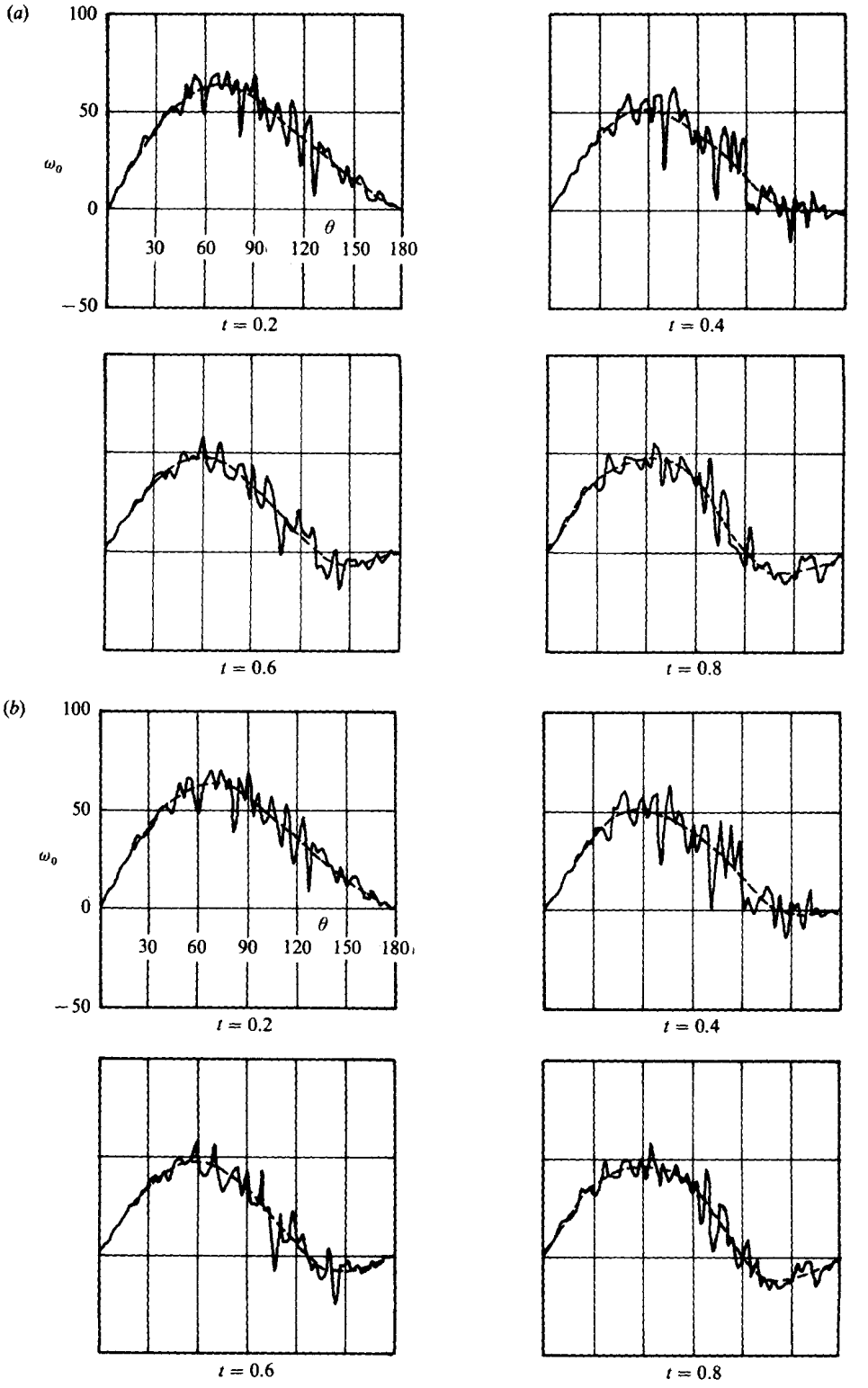


FIGURE 2. Time development of the surface vorticity distribution about a circular cylinder ($n_v = 2$). (*a*) $r_0 = 5$, (*b*) $r_0 = 100$. ——, unsmoothed; – – –, smoothed.

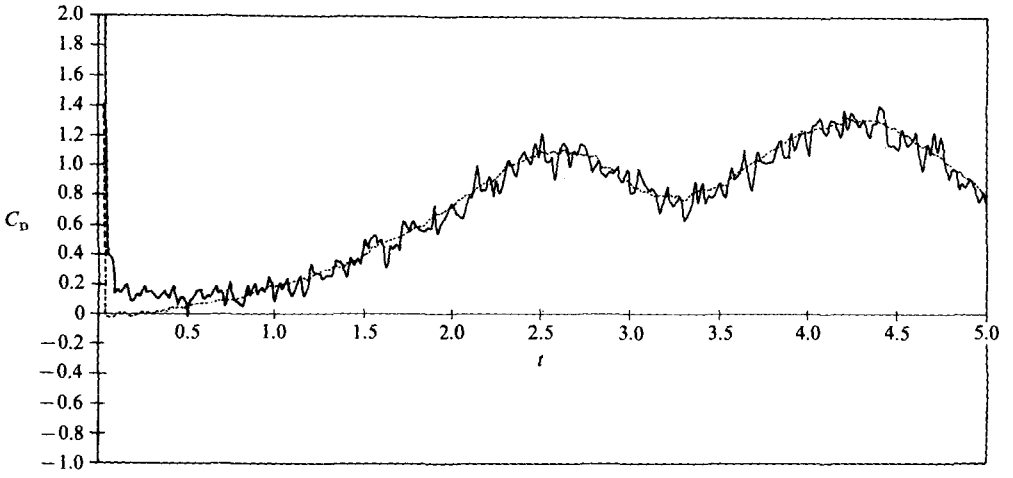


FIGURE 3. Time history of the drag coefficient $C_D$. ——, from (23*a*); - - - -, from (28*a*).

nodes, should therefore be larger on the first timestep than on subsequent steps. $n_v = 20$ was found to be suitable.

Figure 1 shows distributions of $\omega_0$, obtained directly from (25), at $Re = 10^3$ at successive times up to $t = 0.8$. The distributions show a large random component, which can be reduced either by averaging over a number of simulations or, as has been shown here, increasing $n_v$ from 1 to 3 at every timestep (other than the first). A similar random component is present in the surface pressure distributions and force coefficients, and tends to decrease with increasing Reynolds number, as the random walk becomes smaller. The figure also shows the distributions smoothed using a least-squares fit of a fifth-degree polynomial. Increasing $n_v$ has a little effect on these smoothed distributions, although the random component is greatly diminished. $n_v = 2$ was used for all the short-time computations presented in §6. For the longer computations presented in §7, however, larger values of $n_v$ were found to be necessary.

Figure 2 again shows distributions of $\omega_0$ at $Re = 10^3$ at successive times up to $t = 0.8$, both smoothed and unsmoothed. Results using values of $r_0$ of 5 and 100 are compared and show only very slight differences, even in the random component of the distributions. $r_0 = 25$ was used in all the following computations.

Quartepelle & Napolitano (1983) obtained a general formula for the force acting on rigid bodies in incompressible flow, which require a knowledge of the entire vorticity field. For a steady flow past a cylindrical body in the high-Reynolds-number limit (valid for $Re \gtrsim 10^3$), the formula simplifies to the following integral expression for the drag force $f_x$:

$$f_x = \int_v \mathrm{d}V(\boldsymbol{u} \wedge \boldsymbol{\omega}) \cdot \nabla \eta_x, \tag{26}$$

where $V$ is volume and, in the special case of a circular cylinder of unit radius, $\eta_x$ is given by

$$\eta_x = x/r^2. \tag{27}$$

If the vorticity field is discretized using (10), equation (26) gives an expression for the drag coefficient

$$C_D = \sum_{i=1}^{L} \Gamma_i \left[\frac{u_i \sin(2\theta_i) - v_i \cos(2\theta_i)}{r_i^2}\right]. \tag{28a}$$

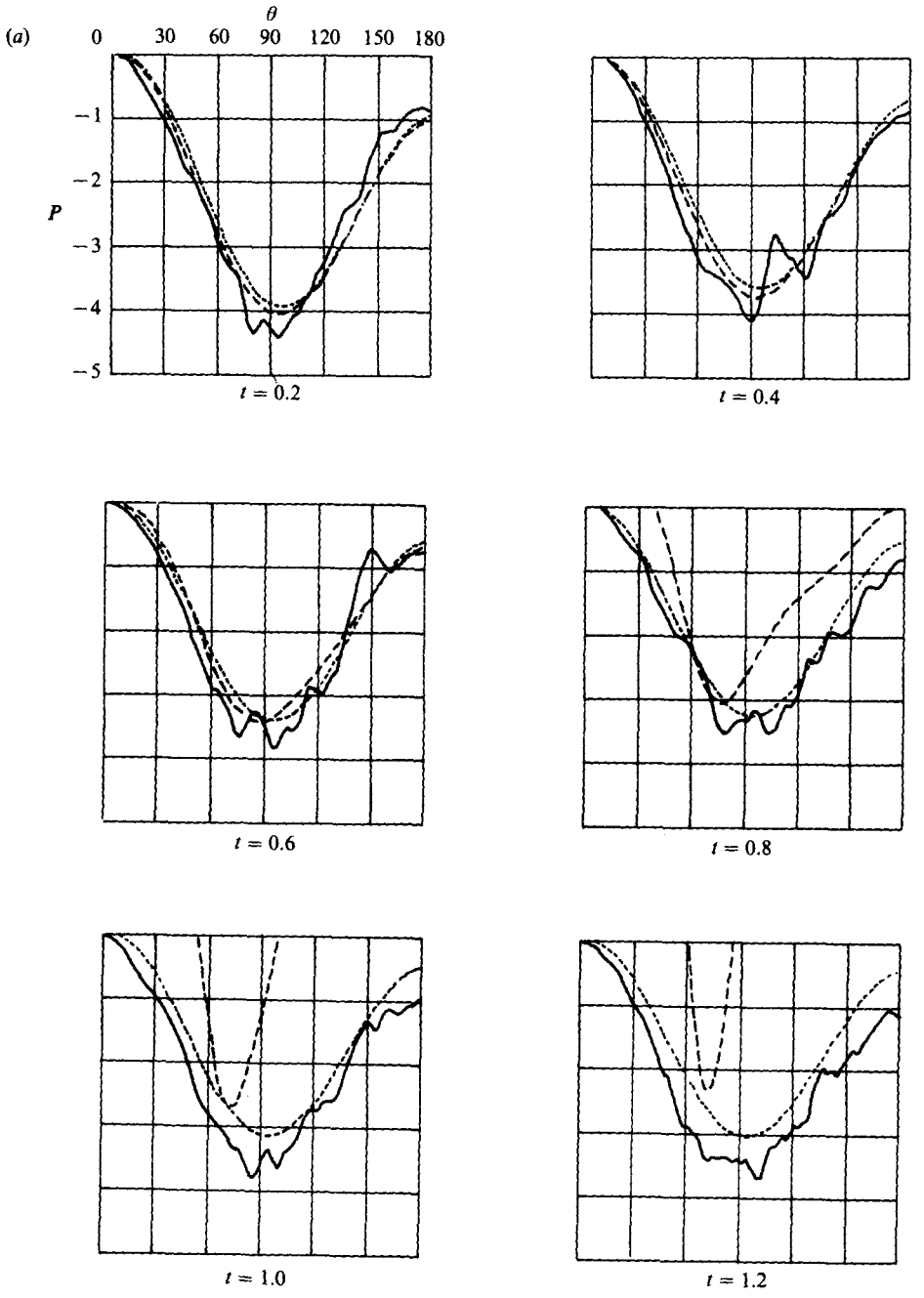


FIGURE 4(a). For caption see page 57.

An analogous expression for the lift coefficient may also be obtained

$$C_{\mathrm{L}} = -\sum_{i=1}^{L} \Gamma_i \left[\frac{v_i \sin(2\theta_i) + u_i \cos(2\theta_i)}{r_i^2}\right], \tag{28b}$$

where the $i$th vortex is at position $\boldsymbol{r}_i = (r_i, \theta_i)$ and has velocity components $u_i$ and $v_i$ parallel to $C_{\mathrm{D}}$ and $C_{\mathrm{L}}$ respectively. A comparison of the force coefficients calculated

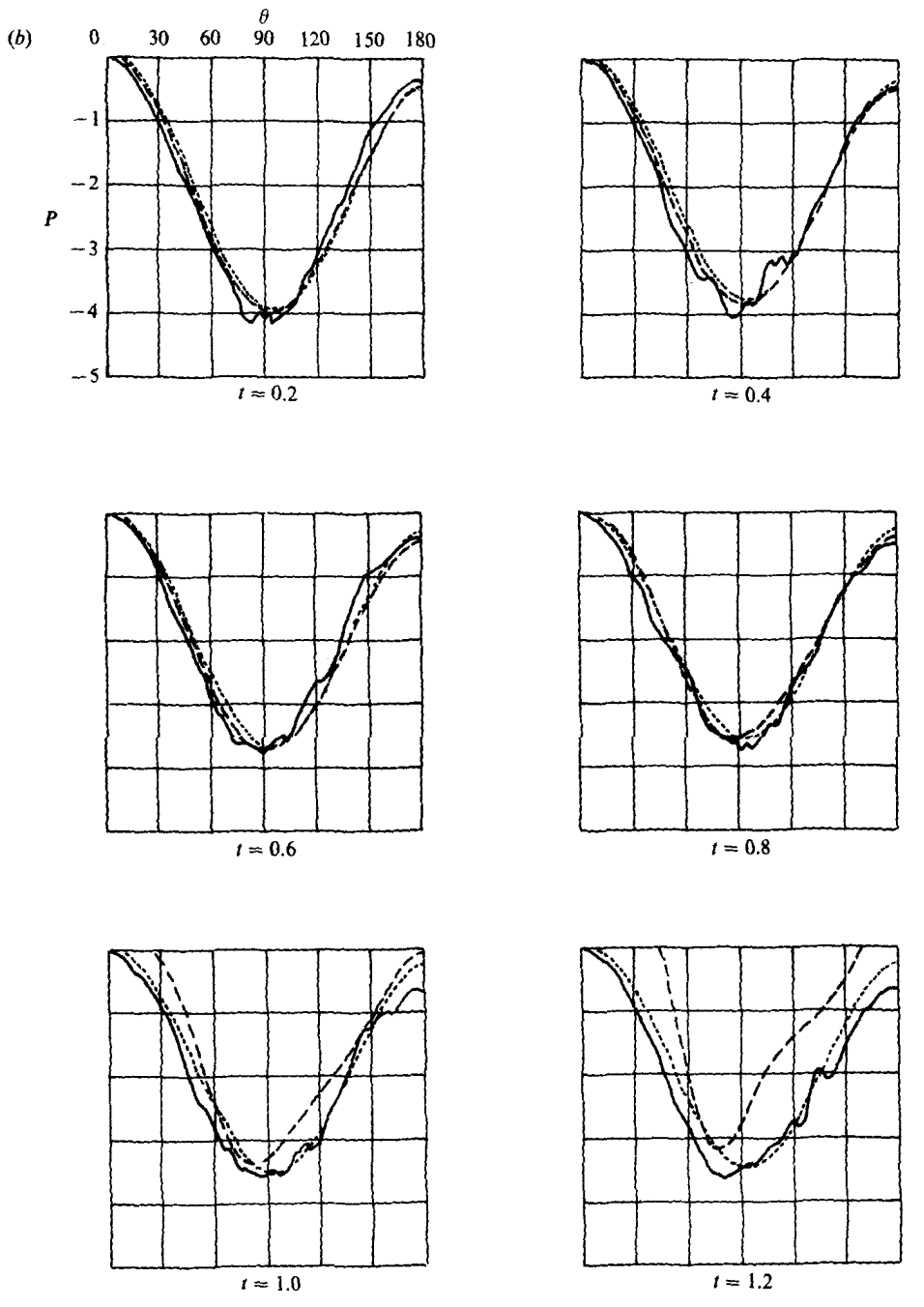


FIGURE 4(*b*). For caption see page 57.

from (23) and (28) provides an internal check on the accuracy of the method; it tests whether the creation of new vortices around the surface of the cylinder, which satisfies the boundary condition on the tangential component of velocity, is consistent with the convection of the vorticity field.

Figure 3 shows a comparison of the time histories of $C_D$ calculated from (23*a*) and (28*a*) at $Re = 10^3$. Agreement is good, although $C_D$ calculated from (23*a*) contains a

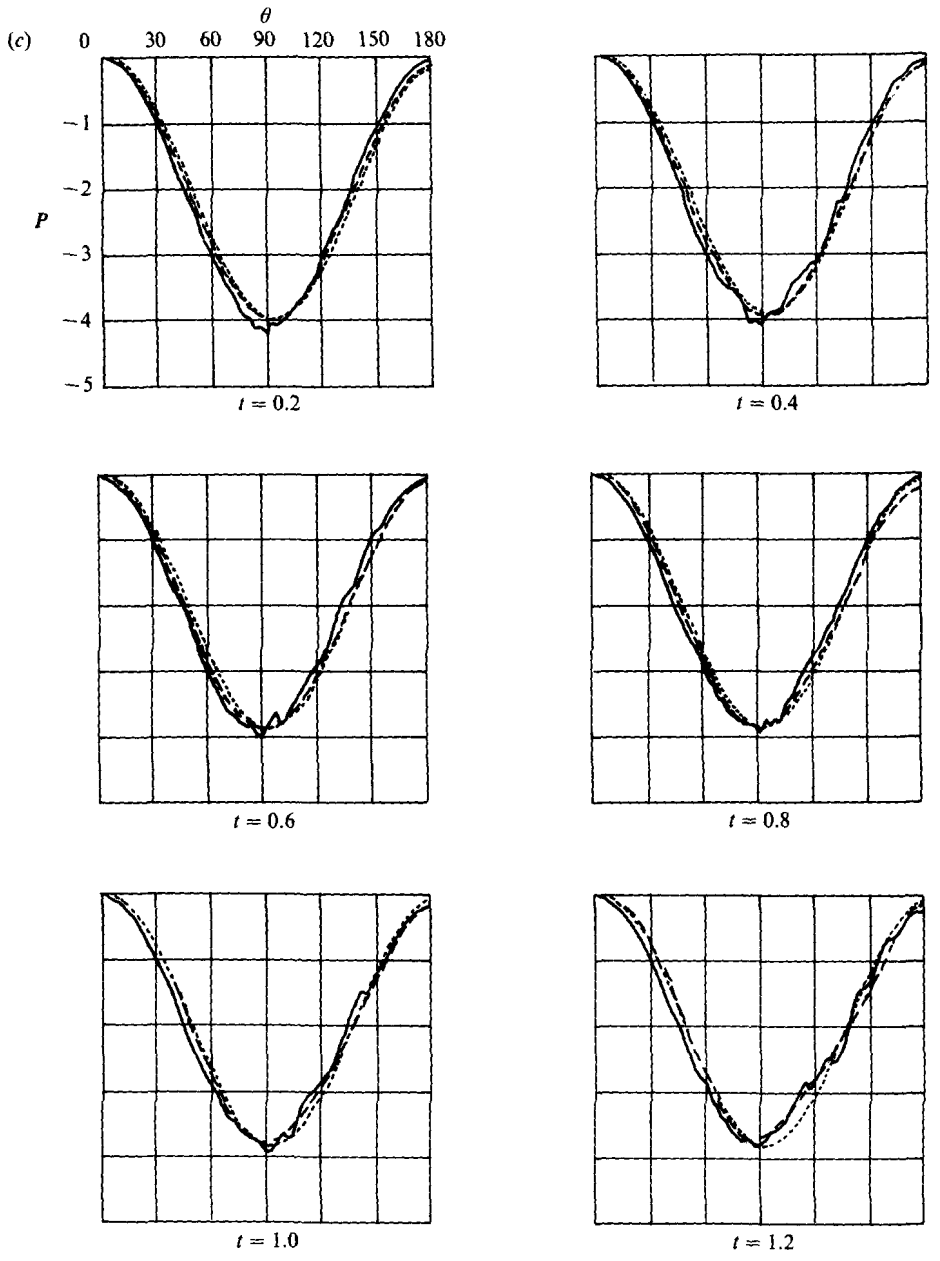


FIGURE 4(c). For caption see facing page.

*random component which is absent in* $C_D$ *calculated from* (28*a*). The quality of the agreement shows little dependence on Reynolds number (above about $10^3$) and improves as the timestep is reduced. A timestep $\Delta t = 0.02$ is shown here, and was used in all the following computations.

## 6. Comparison with power-series solutions

Approximate methods have been developed, which give solutions of (4) and (5), valid over small times following the start of the motion ($t \simeq 0$). The results of two such methods are compared with numerical solutions using the vortex method.

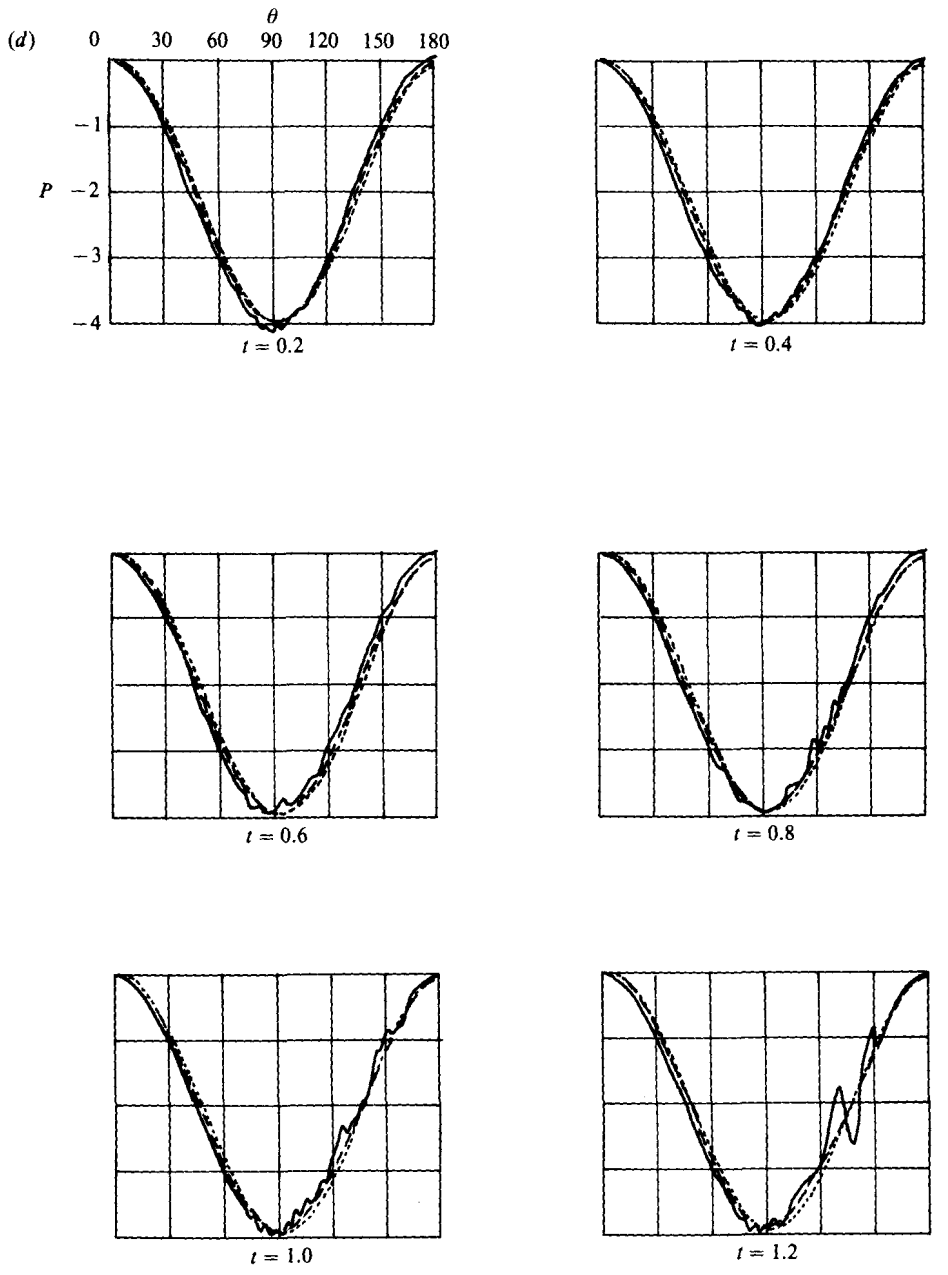


FIGURE 4. Time development of the pressure distribution about a circular cylinder. ——, vortex method; - - - - -, Bar-Lev & Yang (1975); — — —, Collins & Dennis (1973*a*). (*a*) $Re = 2.5 \times 10^2$; (*b*) $Re = 10^3$; (*c*) $Re = 10^4$; (*d*) $Re = 10^5$.

Bar-Lev & Yang (1975) used the method of matched asymptotic expansions. Series solutions to third order in powers of time from $t = 0$ are obtained for the inner (rotational) and outer (potential) flow fields. A composite solution is then formed which is said to be valid for $t < 1$ at $Re \gtrsim 200$ and for $t \approx 1$ at higher Reynolds numbers.

Collins & Dennis (1973*a*) presented a method in which a solution is obtained for

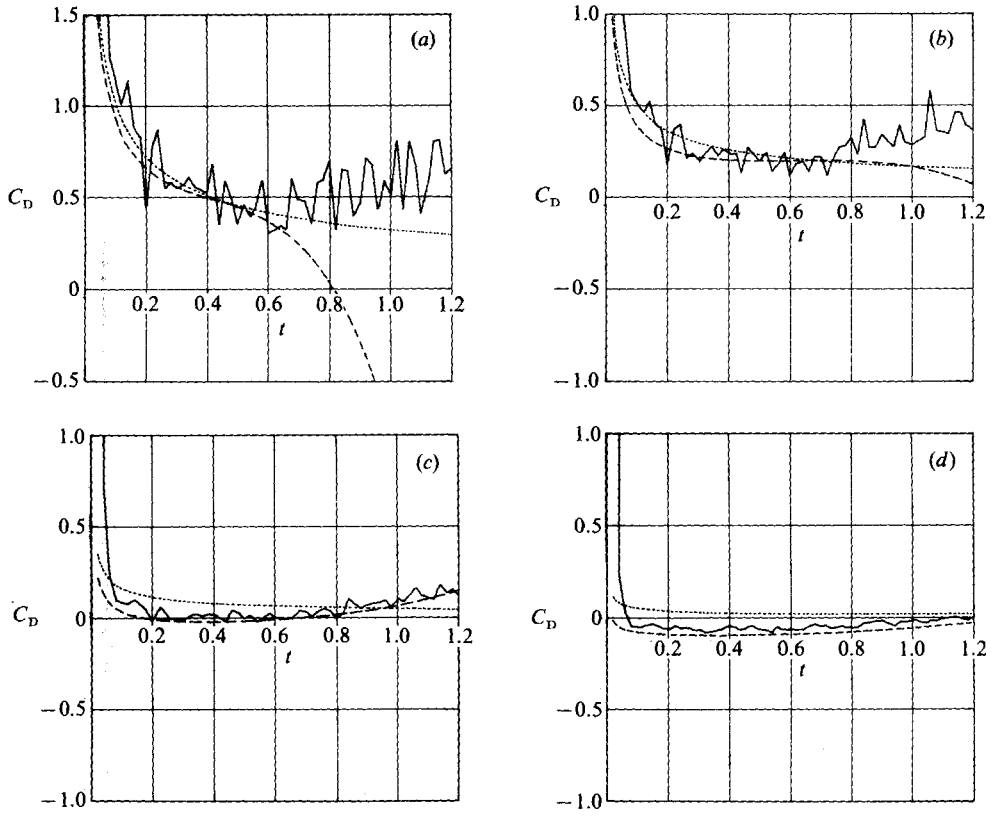


FIGURE 5. Time history of the drag coefficient $C_D$ of a circular cylinder. ——, vortex method; - - - - -, Bar-Lev & Yang (1975); – – –, Collins & Dennis (1973*a*). (*a*) $Re = 2.5 \times 10^2$; (*b*) $Re = 10^3$; (*c*) $Re = 10^4$; (*d*) $Re = 10^5$.

the inner flow field only. This is adjusted so that the flow is uniform at a sufficiently large distance from the cylinder. The solution is a power series in $t$ and a second variable $k = 2(2t/Re)^{\frac{1}{2}}$. Collins & Dennis calculated the solution numerically to seventh order in $t$ and third order in $k$. The results are valid for small $t$ at $Re > 200$. The appropriate range of $t$ is not given precisely, but is known to be $\lesssim 1$ and to increase with Reynolds number.

Flow simulations have been carried out up to $t = 1.2$ across a range of Reynolds numbers. The Reynolds numbers considered are $2.5 \times 10^2$, $10^3$, $10^4$ and $10^5$. The quantities to be compared with power-series solutions are the surface distributions of $P$ and $\omega_0$, calculated at time intervals of 0.2 throughout the simulations, and the time histories of the separation position ($\theta_s$) and drag coefficient ($C_D$). The distributions of $P$ and $\omega_0$ are respectively symmetrical and antisymmetrical about the line $\theta = 0$ and are therefore only presented in the range $0° \leqslant \theta \leqslant 180°$. In the text, the results of the vortex method are denoted by (I), those of Bar-Lev & Yang by (II) and those of Collins & Dennis by (III).

Distributions of $P$ are presented in figure 4 at successive times for each Reynolds number. At $Re = 2.5 \times 10^2$ and $10^3$, agreement between (I), (II) and (III) is reasonable for $t \lesssim 0.6$ and $t \lesssim 0.8$ respectively, bearing in mind that the vortex method has a random component. At later times, (I) and (II) remain in fair

agreement, while (III) clearly becomes invalid. At $Re = 10^4$ and $10^5$, $P$ remains close to the potential flow distribution throughout the period $t \leqslant 1.2$, although a slight increase in $P$ at 90° and a decrease at 180° is shown by all three curves. The increase with Reynolds number of the range of $t$ for which (III) is applicable was predicted by Collins & Dennis.

Figure 5 shows the time history of $C_D$ for each Reynolds number. The impulsive start gives rise to an initially infinite $C_D$, which then decreases rapidly with time. (I) shows $C_D$ to then increase, having reached a minimum value. This minimum becomes smaller and occurs at earlier times as the Reynolds number increases. At $Re = 2.5 \times 10^2$ and $10^3$, agreement between (I), (II) and (III) is again reasonable for $t \lesssim 0.6$, while $C_D$ is decreasing. The subsequent increase in $C_D$ is predicted by neither (II) nor (III), which continue to decrease, although at different rates. At $Re = 10^4$ and $10^5$, fair agreement is obtained between (I) and (III) across the complete range of $t$. At $Re = 10^4$, (II) gives higher values of $C_D$ at $t < 0.9$ and lower values at later times. At $Re = 10^5$, (II) gives consistently higher values of $C_D$.

Figure 6 shows distributions of $\omega_0$, smoothed using the method described in §5. At each Reynolds number, the streamwise gradient of $\omega_0$ at the rearmost point of the cylinder is initially negative, but becomes increasingly positive as the recirculation region develops. At $Re = 2.5 \times 10^2$ and $10^3$, close agreement between (I) and (III) is found for $t \lesssim 0.6$ and $t \lesssim 0.8$ respectively, corresponding with the distributions of $P$ ((II) is unavailable). At $Re = 10^4$ and $10^5$, (I) and (III) show fair agreement across the complete range of $t$, although, for $t \gtrsim 0.8$, there is a tendency for (III) to give minimum values of $\omega_0$ which are more negative than those of (I). These minima, and the zeros of $\omega_0$ on their upstream side, occur nearer to the foremost point of the cylinder in (III) than in (I).

The smoothing of the distributions of $\omega_0$ is important for the location of the separation point, $\theta_s$, taken to be the point at which $\omega_0 = 0$. The zeros of each of the fifth-degree polynomials are plotted against $t$ in order to produce figure 7, graphs of the migration of the separation point for each Reynolds number. Separation first occurs at $t \approx 0.4$ and rapidly progresses upstream. The time taken for separation to first occur becomes smaller as the Reynolds number increases. At $Re = 2.5 \times 10^2$, (III) gives values of $\theta_s$ which are consistently closer to the rearmost point of the cylinder than those of (I), although there is good agreement over the time at which separation first occurs. At $Re = 10^3$ close agreement between (I) and (III) is found across the complete range of $t$. At $Re = 10^4$ and $10^5$, when $t \gtrsim 0.8$, there is a tendency for (III) to give values of $\theta_s$ which are nearer to the foremost point of the cylinder than those of (I). This feature has already been noted in the distributions of $\omega_0$ (figure 6).

## 7. Comparison with finite-difference solutions and flow visualizations

Eulerian finite-difference schemes have also been applied to the starting flow around a circular cylinder. The results of two accurate schemes without upwind differencing, presented by Collins & Dennis (1973*b*) and Ta Phuoc Loc & Bouard (1985), are compared with the results of the Lagrangian vortex method. Following Ta Phuoc Loc & Bouard, a comparison is also made between the numerical results and the flow-visualization experiments of Bouard & Coutanceau (1980).

Collins & Dennis presented integrations of the Navier–Stokes equations over a range of Reynolds numbers from 5 to $\infty$. They give results up to the time at which

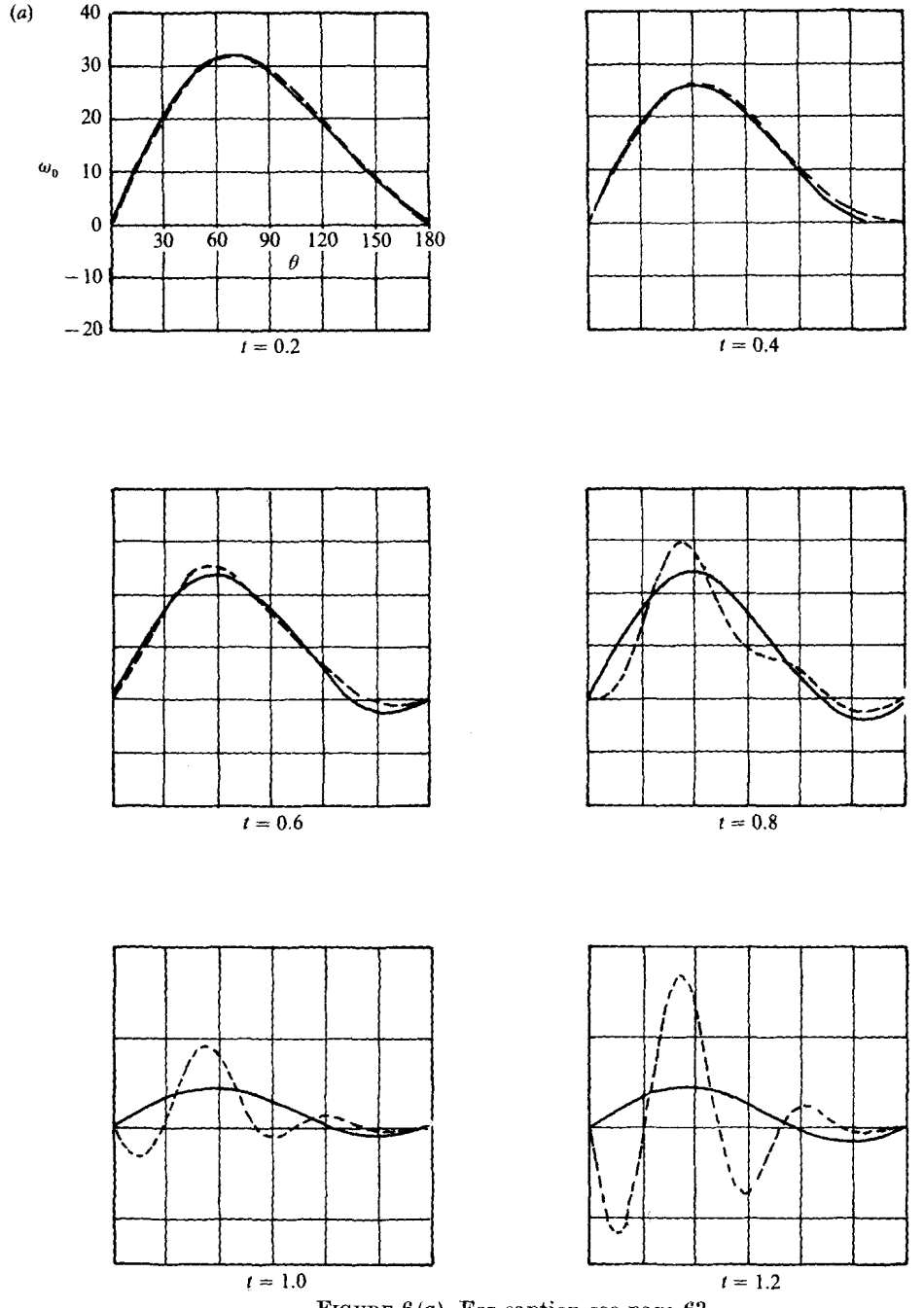


FIGURE 6(a). For caption see page 63.

their implicit method of integration failed to converge. This time is generally greater than the period for which the series solutions (Collins & Dennis 1973*a*) are valid, but decreases as the Reynolds number is increased.

Figure 8 shows a comparison of the development of the streamline patterns up to $t = 4.8$ at $Re = 500$, at which stage the integration of Collins & Dennis broke down. The flows are again symmetrical about the line $\theta = 0°$ and, for simplicity, only one

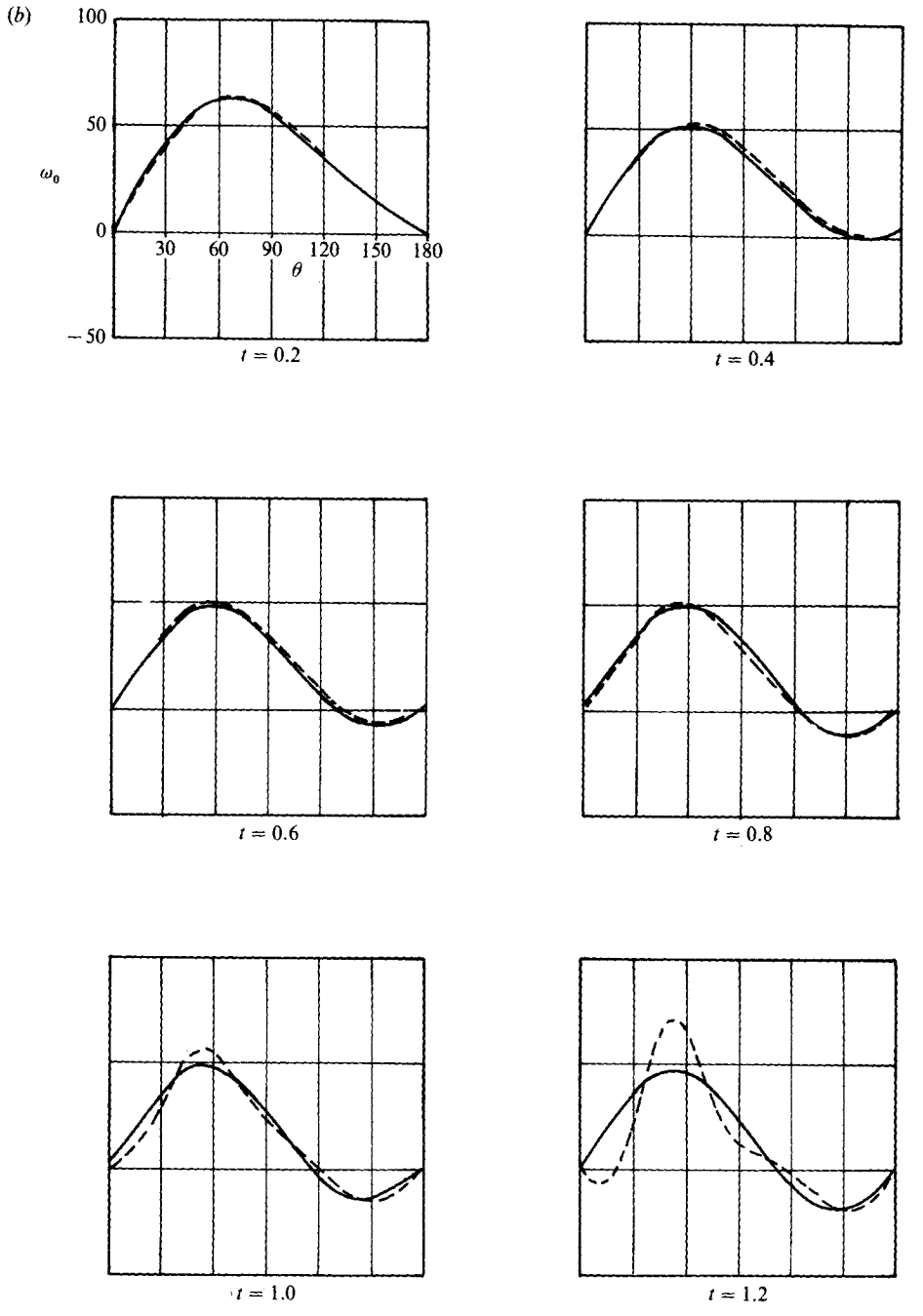


FIGURE 6(*b*). For caption see page 63.

half of each flow will be reproduced. There is, in general, good agreement between the two numerical methods. Both show the elongation with time of the primary eddy and the appearance of a secondary eddy on the surface of the cylinder at a time between $t = 2.0$ and $t = 3.2$. The figure also shows the streamline $\psi = 0$, taken from the results of Collins & Dennis, superimposed on the streamlines from the vortex method. The positions of the secondary eddies are in close agreement and there is reasonable

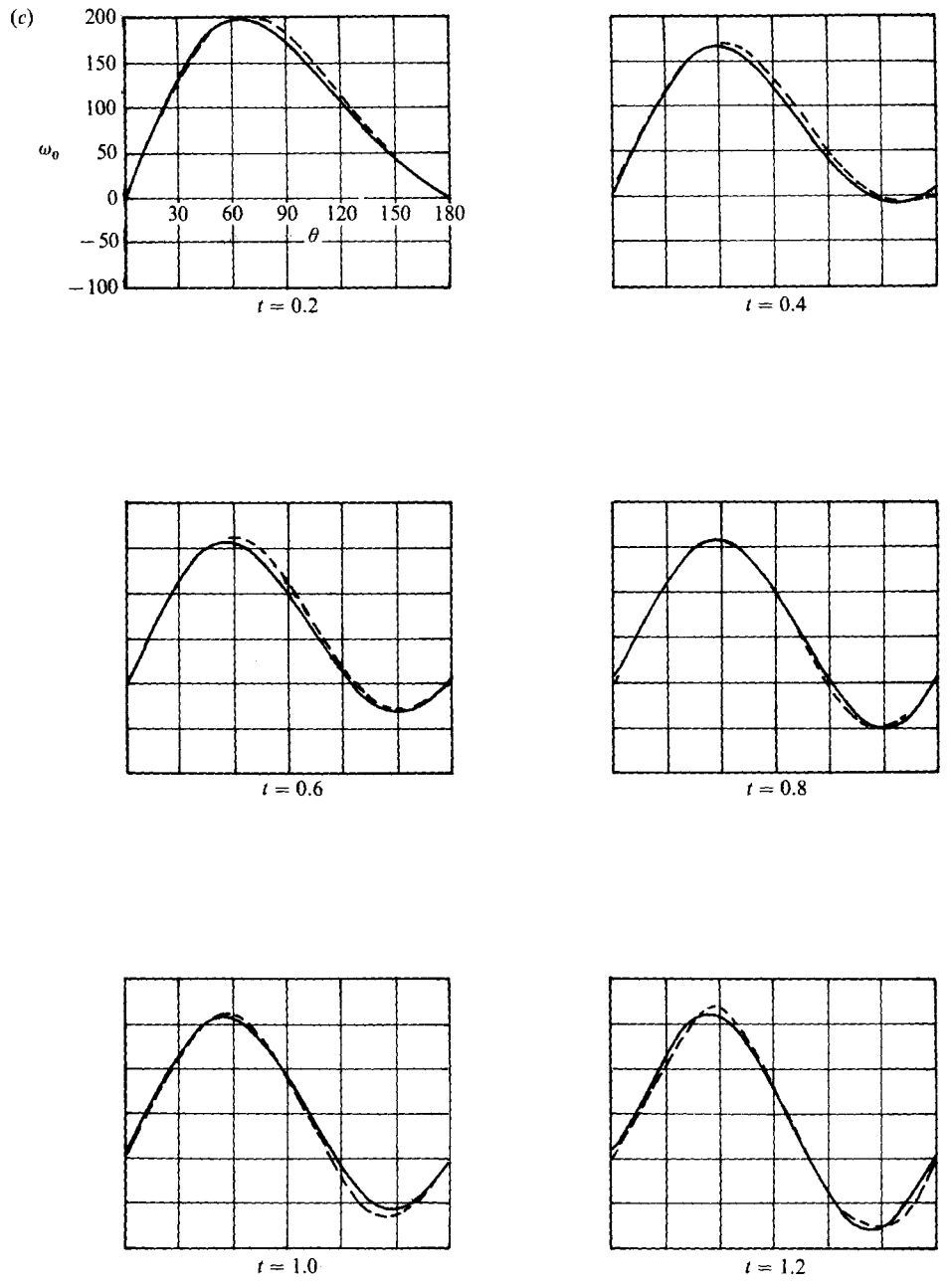


FIGURE 6(c). For caption see facing page.

agreement in the shape of the primary eddies. At $t = 3.2$ and $t = 4.0$, however, the primary eddy of Collins & Dennis is slightly larger than that of the vortex method The results of the vortex method were found to be insensitive to refinement of the mesh, to increase in $n_v$ and to reduction in $\Delta t$.

Bouard & Coutanceau (1980) presented a series of flow visualization experiment for $t \leqslant 5$ and $Re < 10^4$. Ideal starting flows are closely approximated in thes experiments; the distant flow reaches its final velocity at $t \leqslant 0.04$ $(= 2\,\Delta t)$.

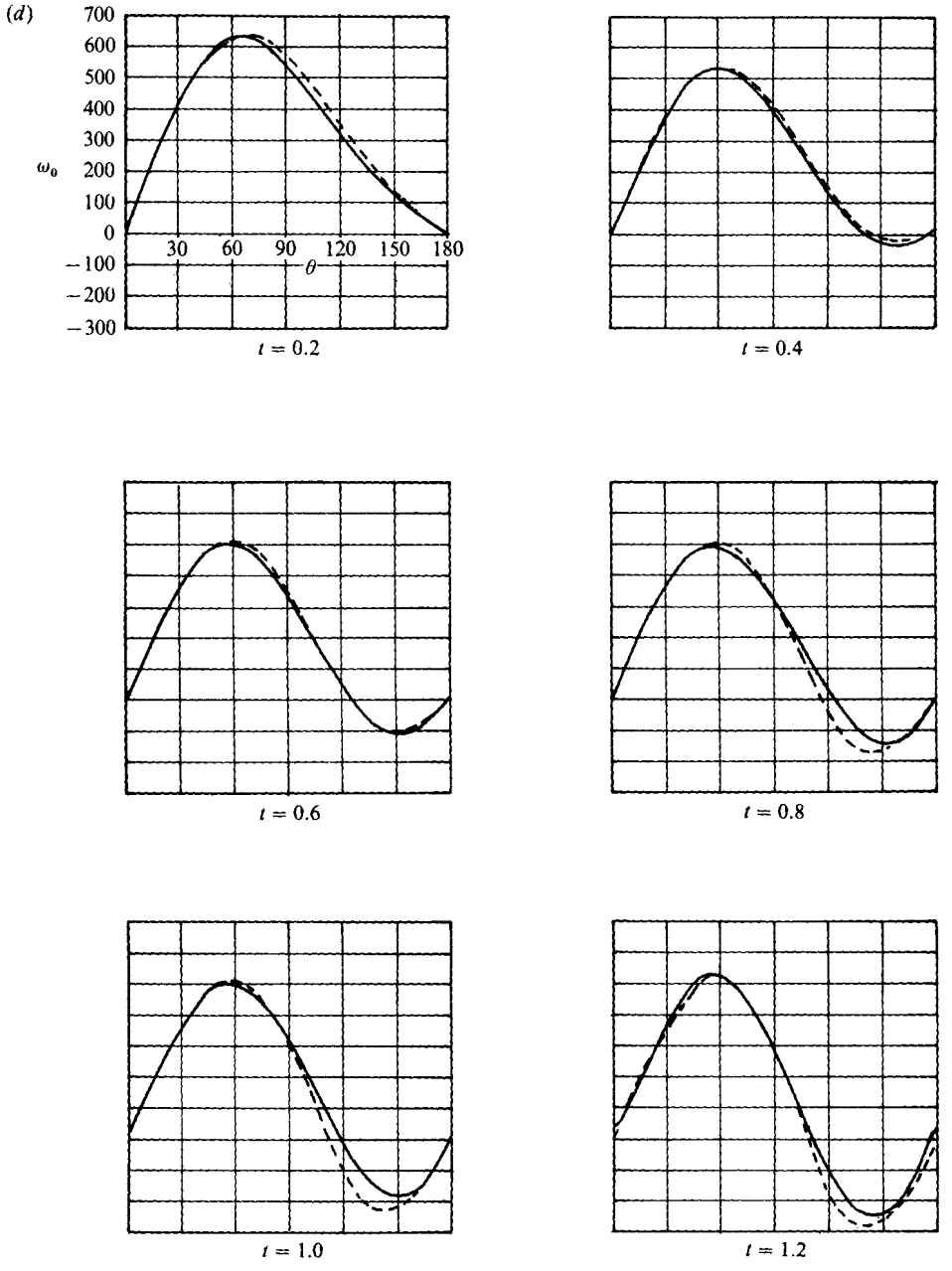


FIGURE 6. Time development of the surface vorticity distribution about a circular cylinder. ——, vortex method; – – –, Collins & Dennis (1973*a*). (*a*) $Re = 2.5 \times 10^2$; (*b*) $Re = 10^3$; (*c*) $Re = 10^4$; (*d*) $Re = 10^5$.

Figures 9 and 10 compare real fluid flows, visualized using tracer particles, with the results of the vortex method, again presented in the form of streamline patterns. They show the flow at $t = 5$, $Re = 300$ and $Re = 550$. The 'bulge phenomenon' described by Bouard & Coutanceau, a distortion in the streamlines at about $\vartheta = 135°$, appears in both the experimental and numerical flow patterns although, at $Re = 300$, it is not well resolved by the numerical method.

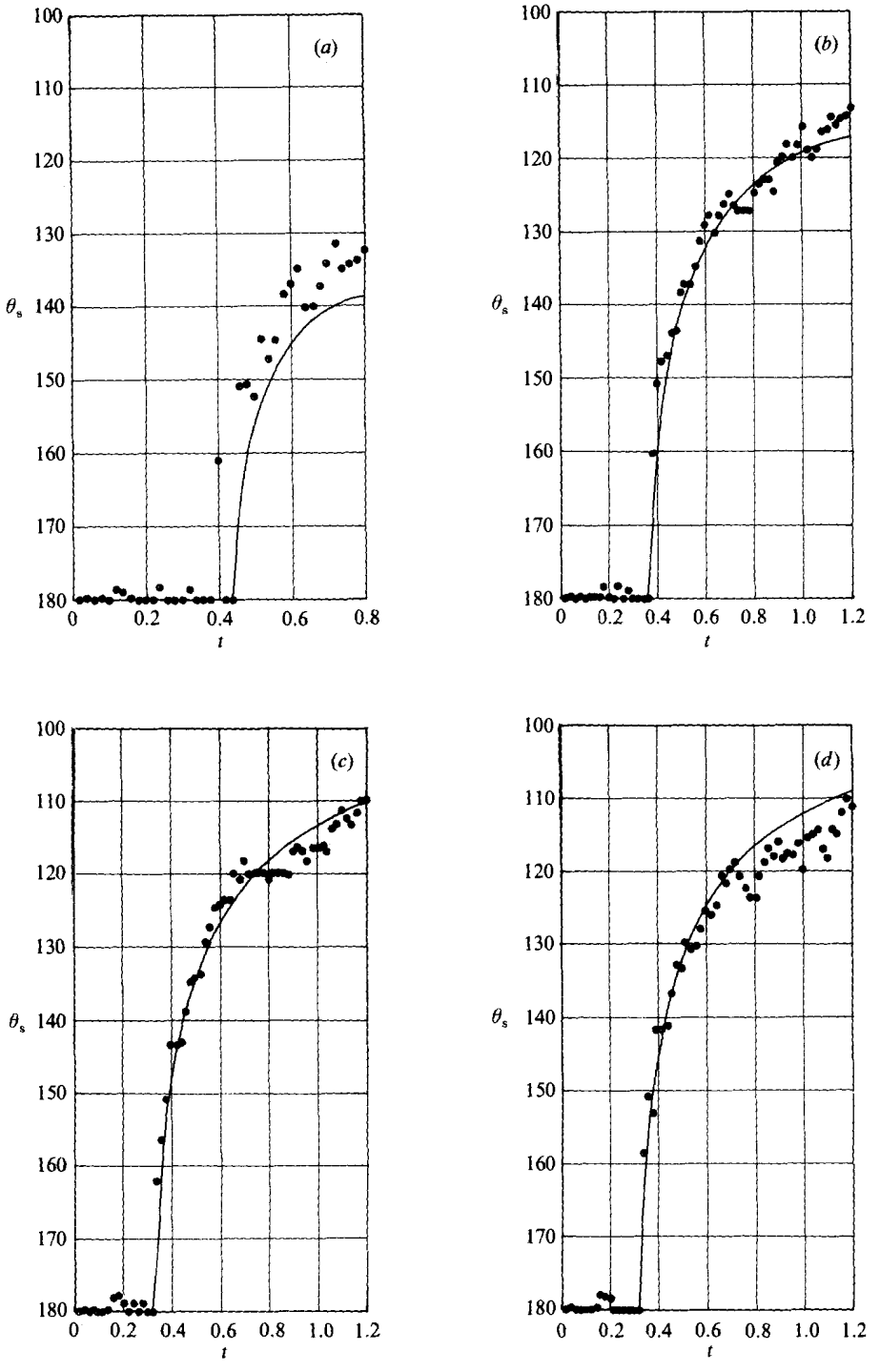


FIGURE 7. Time history of the separation point. ●, vortex method; ——, Collins & Dennis (1973*a*). (*a*) $Re = 2.5 \times 10^2$; (*b*) $Re = 10^3$; (*c*) $Re = 10^4$; (*d*) $Re = 10^5$.

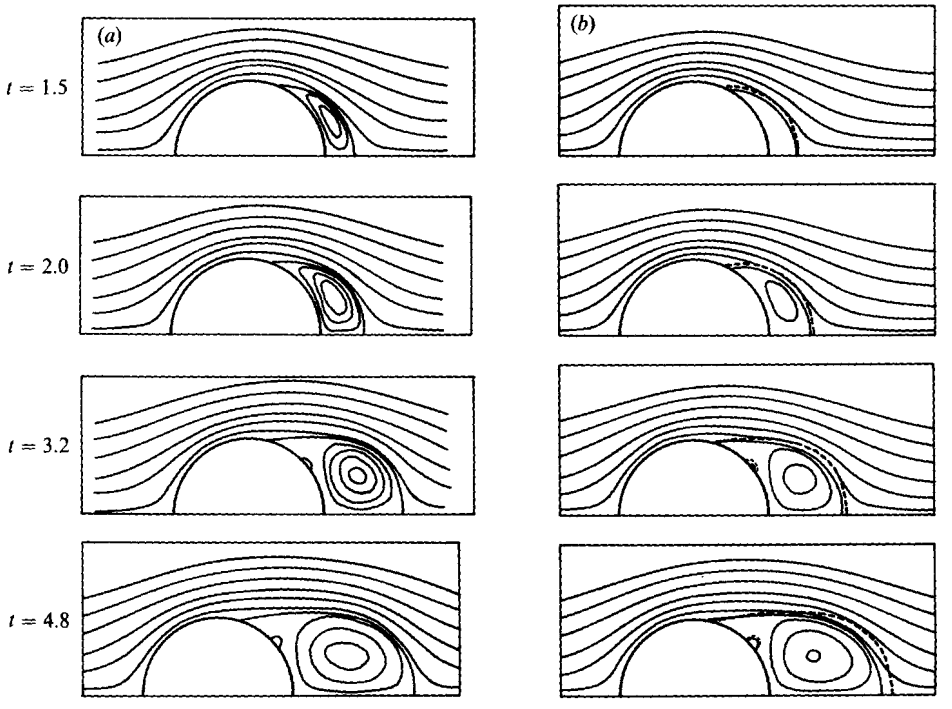


FIGURE 8. Comparison of the development of the streamline patterns from two numerical methods. (*a*) Collins & Dennis (1973*b*); (*b*) Vortex method. ——, the streamline $\psi = 0$ from the results of Collins & Dennis.

Ta Phuoc Loc & Bouard (1985) presented integrations of the Navier–Stokes equations at Reynolds numbers of 3000 and 9500 and compared their results with the flow visualizations of Bouard & Coutanceau. Figures 11–14 show a comparison of these results with those of the vortex method.

Figure 11 gives profiles of the radial velocity on the symmetry axis behind the cylinder up to $t = 5$ at $Re = 3000$. For clarity, only the experimental results and the results of the vortex method are shown in this figure (the numerical results of Ta Phuoc Loc & Bouard were in good agreement with the experimental data). The results of the vortex method were again found to be insensitive to refinement of the mesh and to reduction in $\Delta t$, but are sensitive to an increase in $n_v$. Generally, as $t$ increases, a larger value of $n_v$ is required for convergence. $n_v = 5$ was the largest practical value for these simulations, and the results may be considered reliable up to a time between $t = 3$ and $t = 4$.

Figure 12 shows successive flow patterns up to $t = 5$ at $Re = 3000$, using $n_v = 5$ in the vortex method. There is good qualitative agreement between the results of the two numerical methods and the experimental visualizations. The distortion in the streamlines, noted in figures 9 and 10, develops into an isolated secondary eddy, and is sufficiently large to separate a further secondary eddy from the main recirculating region: 'phenomenon $\alpha$' of Bouard & Coutanceau.

Figure 13 gives profiles of the radial velocity on the symmetry axis behind the cylinder up to $t = 4$ at $Re = 9500$. Again, the vortex method gave results which were sensitive to an increase in $n_v$, with larger values of $n_v$ required for convergence as $t$

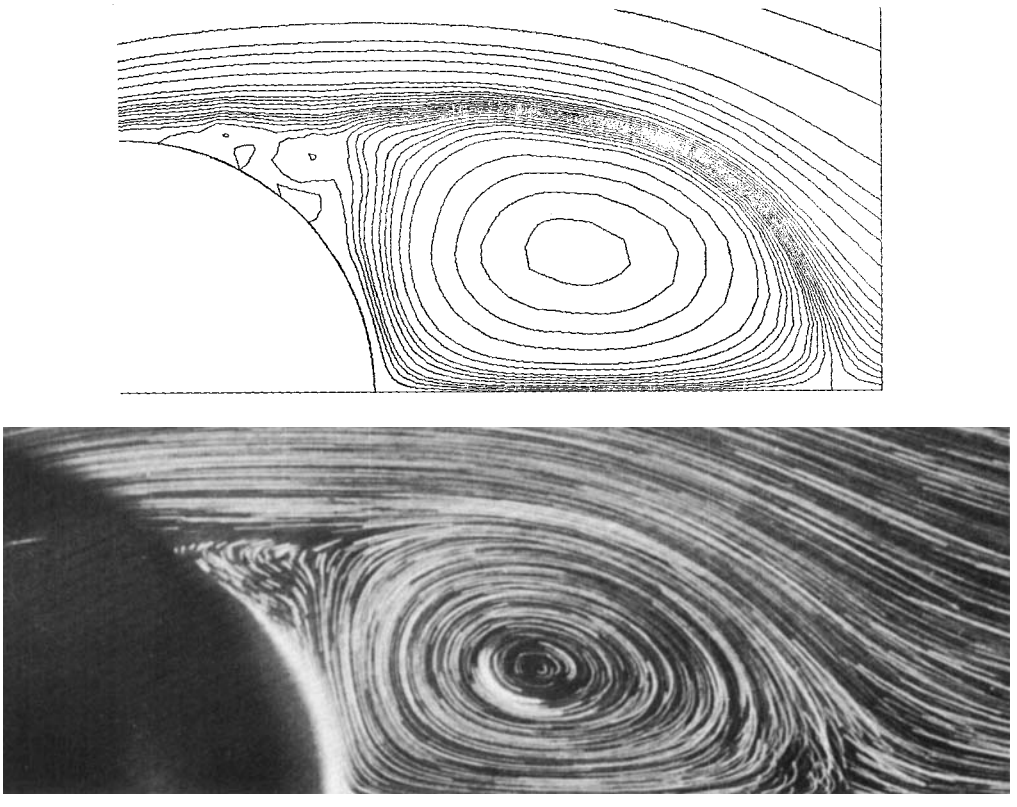

FIGURE 9. Comparison of the experimental flow visualizations of Bouard & Coutanceau (1980) with streamlines from the vortex method at $t = 5$, $Re = 300$.

increases. With $n_v = 6$, the results may be considered reliable up to a time between $t = 2$ and $t = 2.8$.

Figure 14 shows successive flow patterns up to $t = 4$ at $Re = 9500$, using $n_v = 6$ in the vortex method. At $t = 1.6$, the recirculating wake is confined to a thin layer adjacent to the cylinder surface, with a rapidly rotating core resolved by both numerical methods. At $t = 2.8$, the core develops into the primary eddy. There are also two secondary eddies on the surface of the cylinder, again resolved by both numerical methods. At later times, the numerical methods give diverging results, as expected from figure 13. However, it is noted that, in the experiment, the paths of the tracer particles intersect each other in the wake, indicating a rapid change in the flow pattern; Bouard & Coutanceau state that the flow becomes unstable immediately after $t = 4.0$.

## 8. Discussion and conclusions

The starting flow around a circular cylinder has been computed using a Lagrangian vortex method, in which particular attention has been paid to the surface conditions. The time variation of surface pressure and surface vorticity distributions, separation positions, forces, streamline patterns and velocities in the near wake have been compared, where possible, with two analytical time-series solutions, two Eulerian

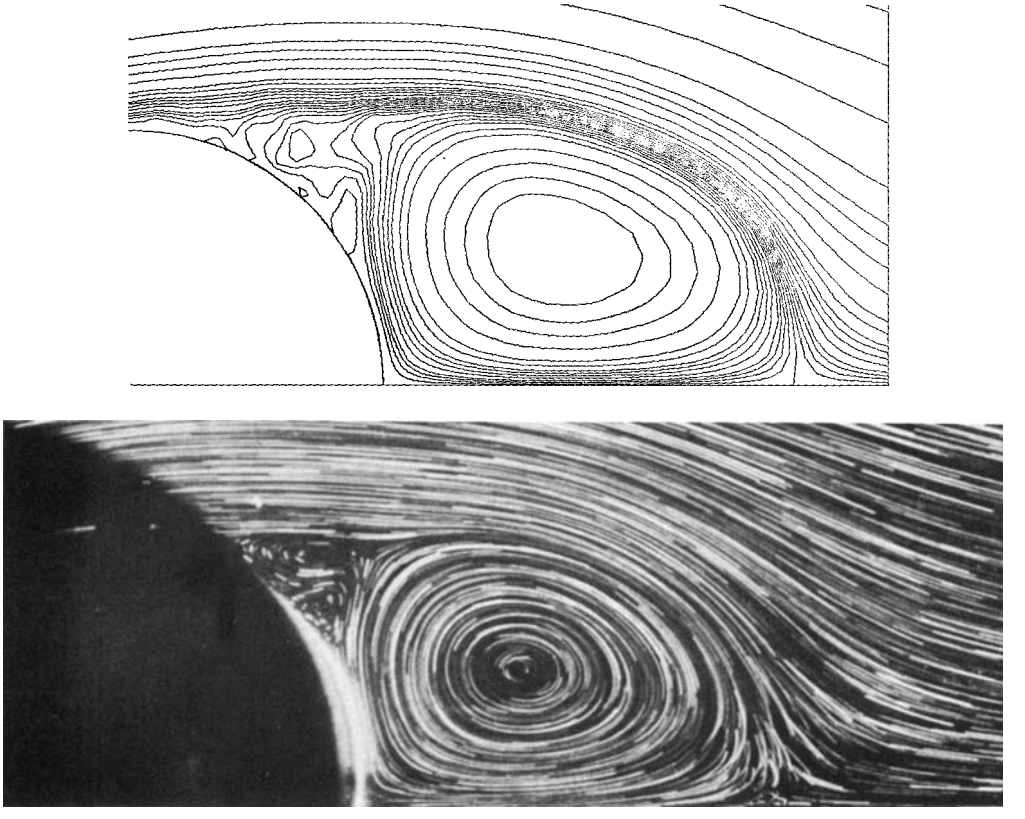

FIGURE 10. Comparison of the experimental flow visualizations of Bouard & Coutanceau (1980) with streamlines from the vortex method at $t = 5$, $Re = 550$.

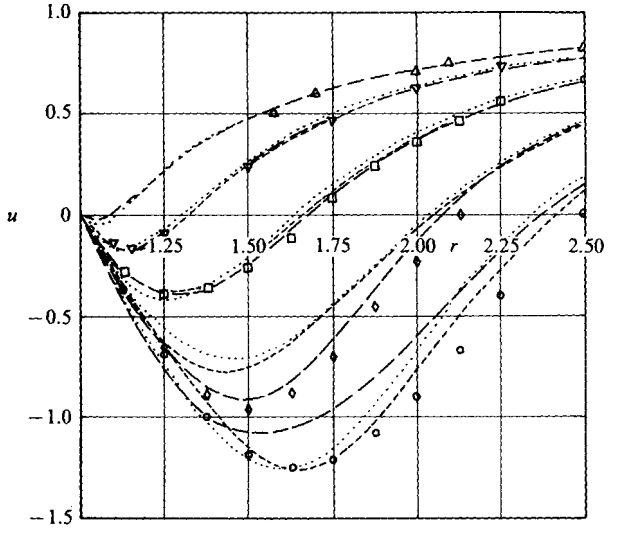


FIGURE 11. The radial velocity on the symmetry axis behind the cylinder at $Re = 3000$. Experimental data (Ta Phuoc Loc & Bouard 1985): △, $t = 1$; ▽, $t = 2$; □, $t = 3$; ◇, $t = 4$; ○, $= 5$. Vortex method: · · · ·, $n_v = 3$; ——, $n_v = 4$; ————, $n_v = 5$.

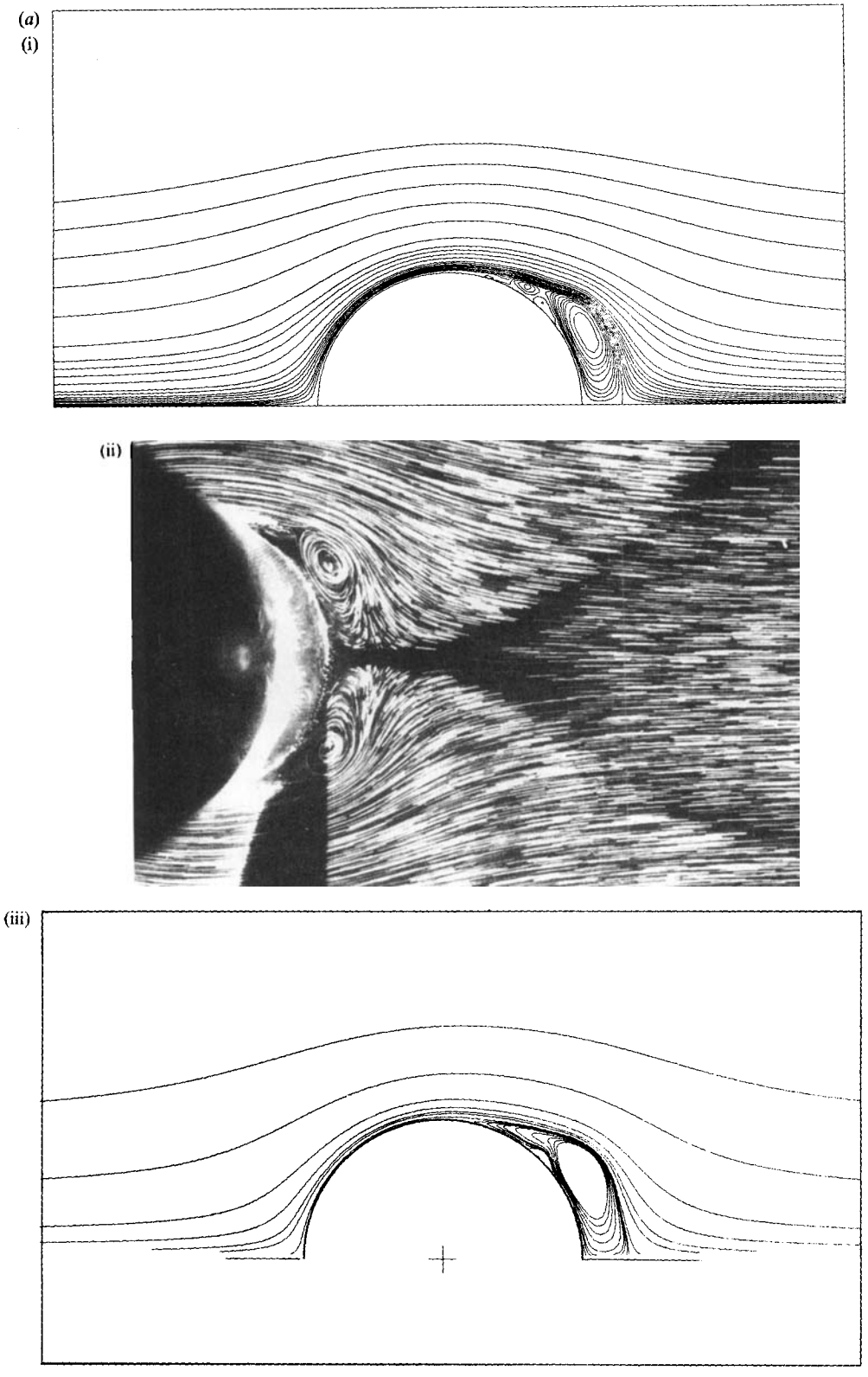


FIGURE 12(*a*). For caption see page 71.

(*b*)
(i)

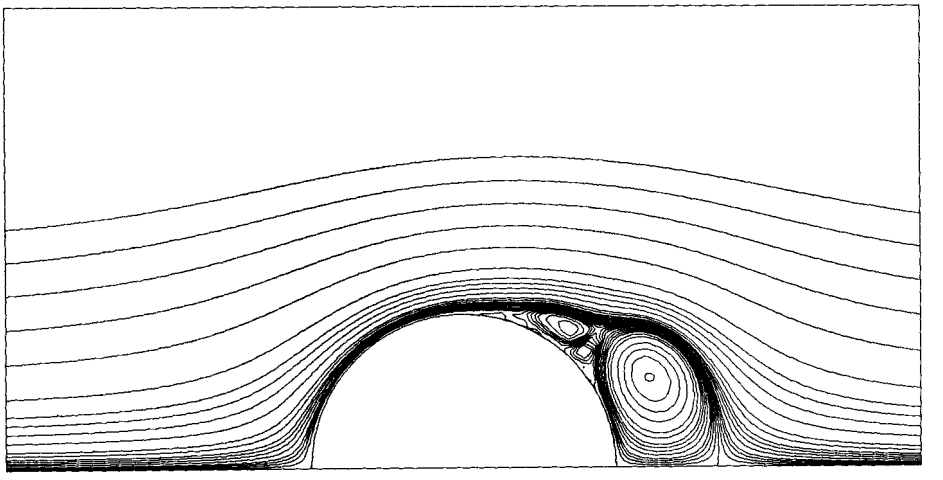

(ii)

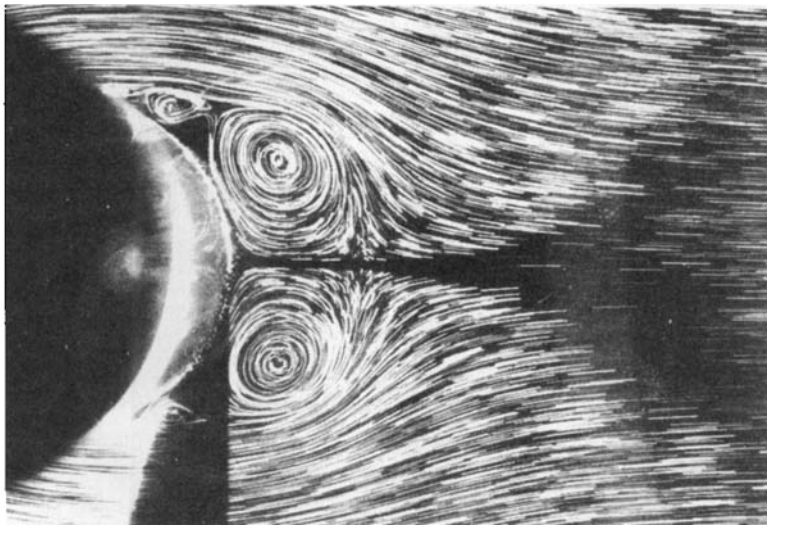

(iii)

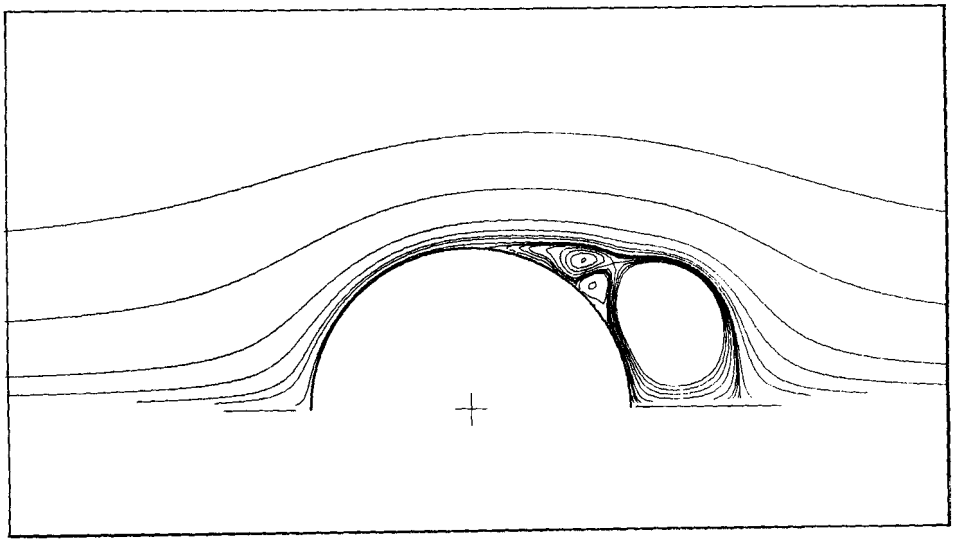

FIGURE 12(*b*). For caption see page 71.

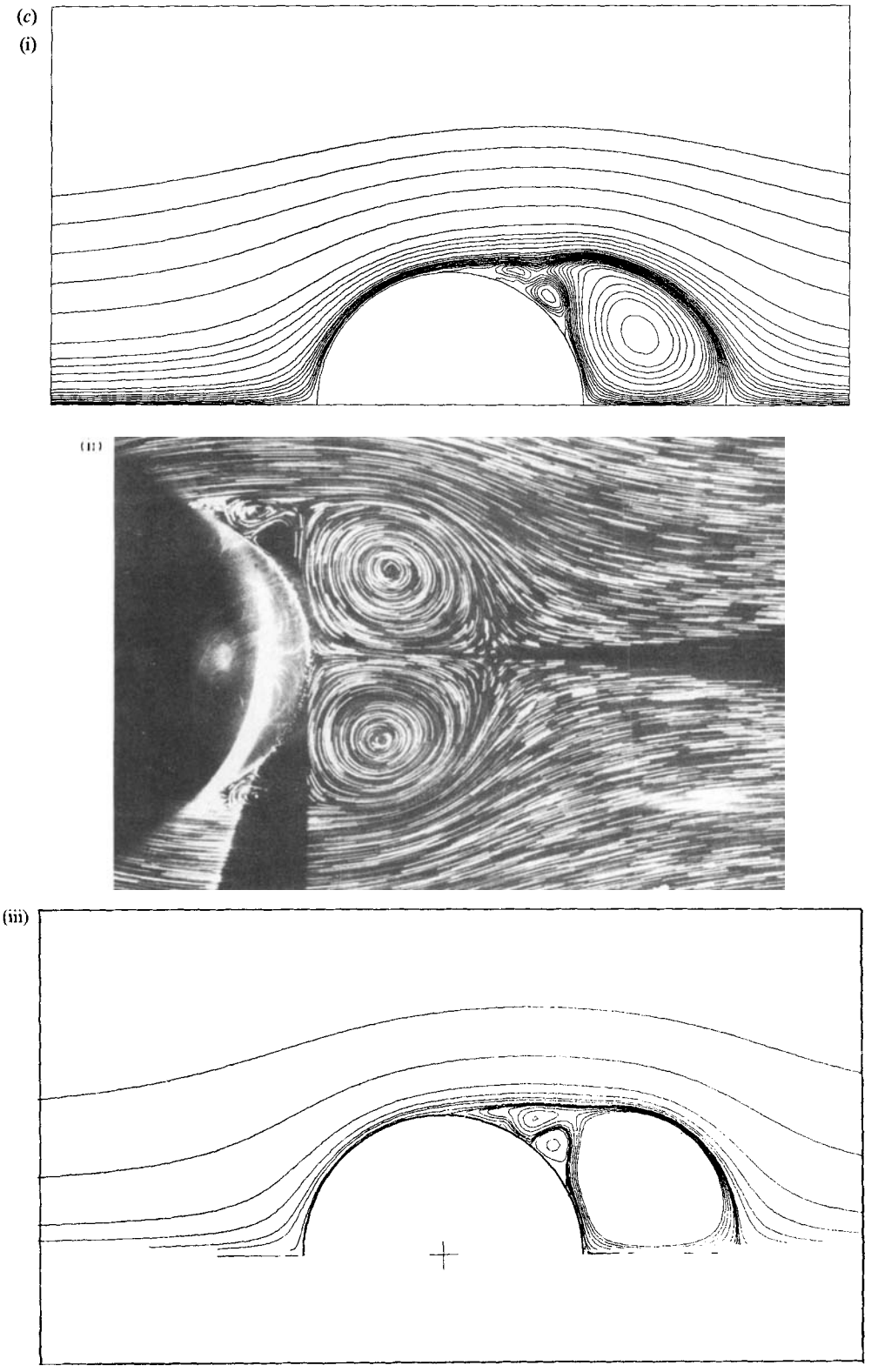


FIGURE 12(*c*). For caption see facing page.

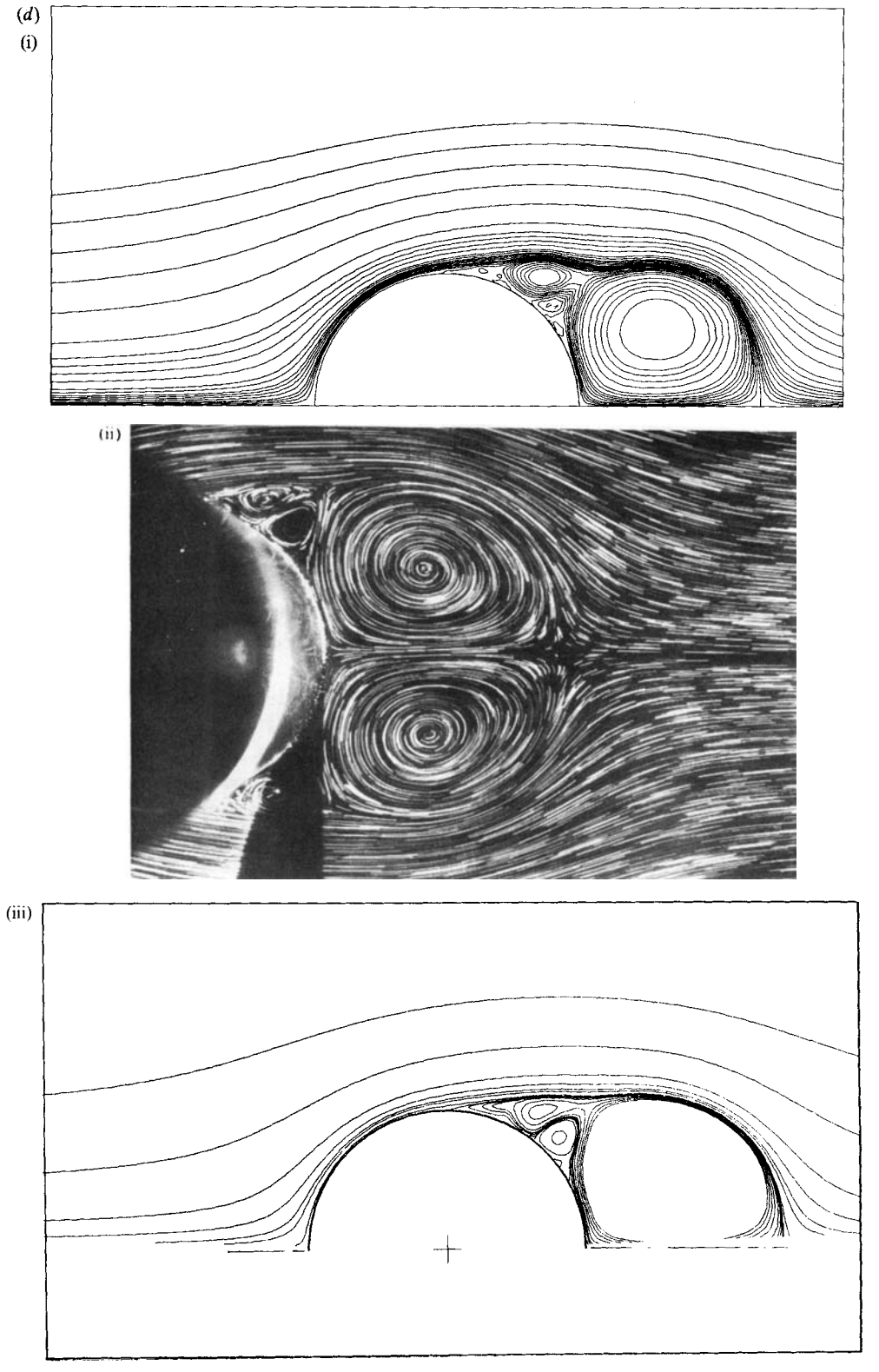


FIGURE 12. Comparison at $Re = 3000$ of the streamlines from the vortex method (i) with experimental visualizations (ii) and with streamlines from a finite-difference method (iii) (Ta Phuoc Loc & Bouard 1985). (*a*) $t = 2$; (*b*) $t = 3$; (*c*) $t = 4$; (*d*) $t = 5$.

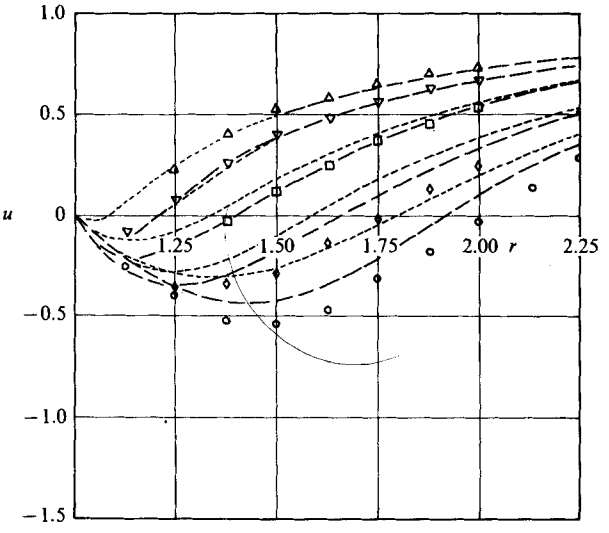


FIGURE 13. The radial velocity on the symmetry axis behind the cylinder at $Re = 9500$. Experimental data (Ta Phuoc Loc & Bouard 1985): △, $t = 1.2$; ▽, $t = 2.0$; □, $t = 2.8$; ◇, $t = 3.6$; ○, $t = 4.0$. Vortex method: -----, $n_v = 5$; ——, $n_v = 6$.

finite-difference schemes and some careful experiments, giving a comprehensive description of the flow.

There is close agreement between the results of the vortex method and those of the finite-difference methods of Collins & Dennis (1973*b*) and Ta Phuoc Loc & Bouard (1985). The large primary eddies and the secondary eddies are both well predicted.

Variation of the numerical parameters in the vortex method and comparison with the velocities in the near wake presented by Ta Phuoc Loc & Bouard, which are in close agreement with experiment, show that the number of vortices in the flow is a vital parameter for convergence. Accurate velocity predictions require more vortices per timestep for longer than for shorter runs and for higher than for lower Reynolds numbers. If too few are introduced, the primary eddies in the wake tend to roll up too tightly. Since convection dominates vorticity diffusion away from the surface at high Reynolds numbers, the large number of vortices appears to be necessary for an accurate vortex-in-cell calculation. Convergence with a smaller number of vortices might be possible using a vortex-blob method with high-order core structures (Anderson & Greengard 1985). Incorporation of this through local corrections in the vortex-in-cell method could be considered (Anderson 1986).

The migration of the separation points is a prominent characteristic of the flow development, but this could only be compared with the time-series solution of Collins & Dennis (1973*a*). Agreement was good for Reynolds numbers of $2.5 \times 10^2$ and $10^3$ but was less satisfactory at $10^4$ and $10^5$. This is possibly related to the formation of small-scale eddy structures ahead of separation at very high Reynolds numbers.

The starting flow around a circular cylinder is a valuable benchmark test for a two-dimensional, viscous-flow computation method. The flow has highly transient characteristics which are now well defined. It would be useful, however, to check the velocity measurements using modern equipment, since Bouard & Coutanceau obtained these by simply measuring the displacements of tracer particles on a photographic plate.

The vortex method in the form used here is thus capable of accurately predicting

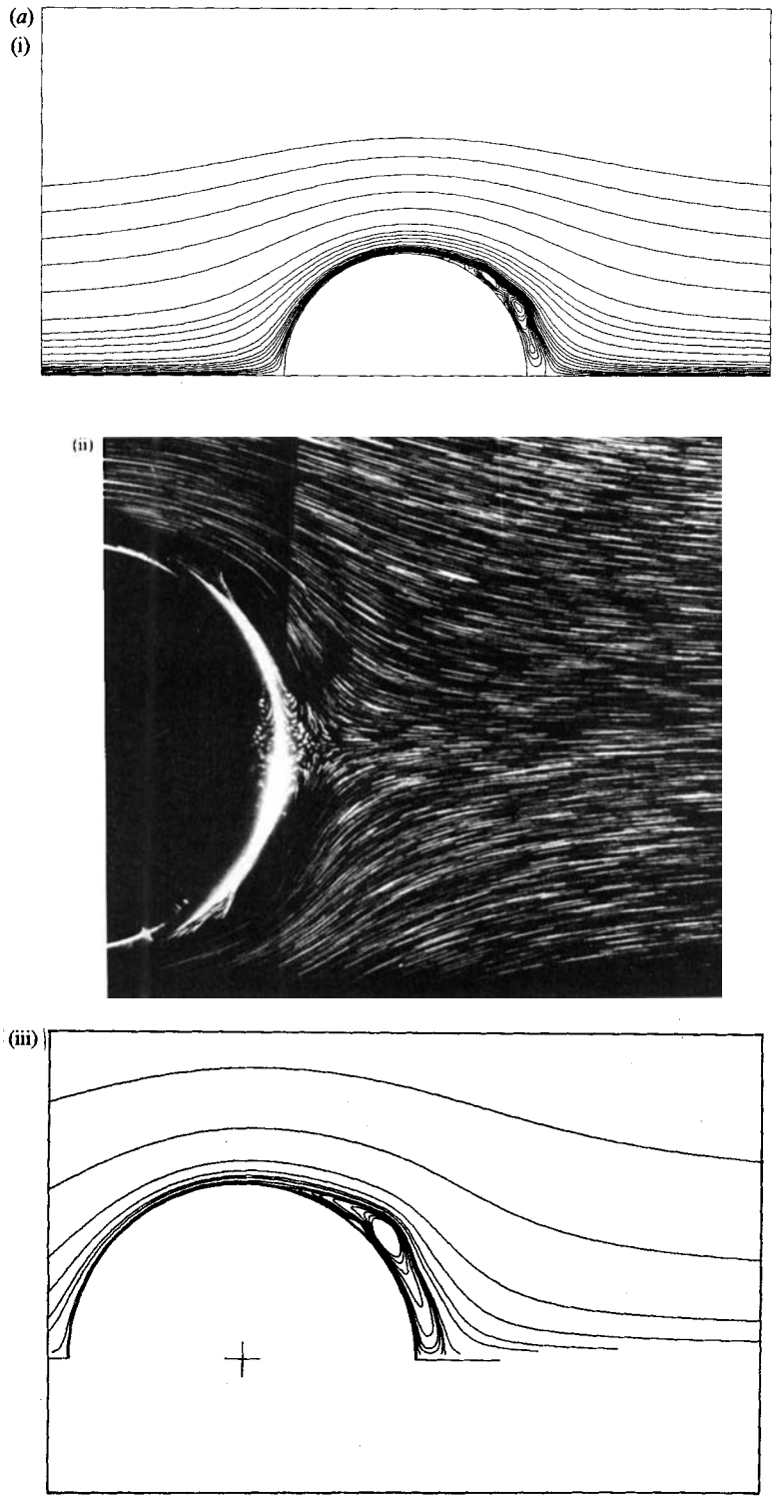


FIGURE 14(*a*). For caption see page 76.

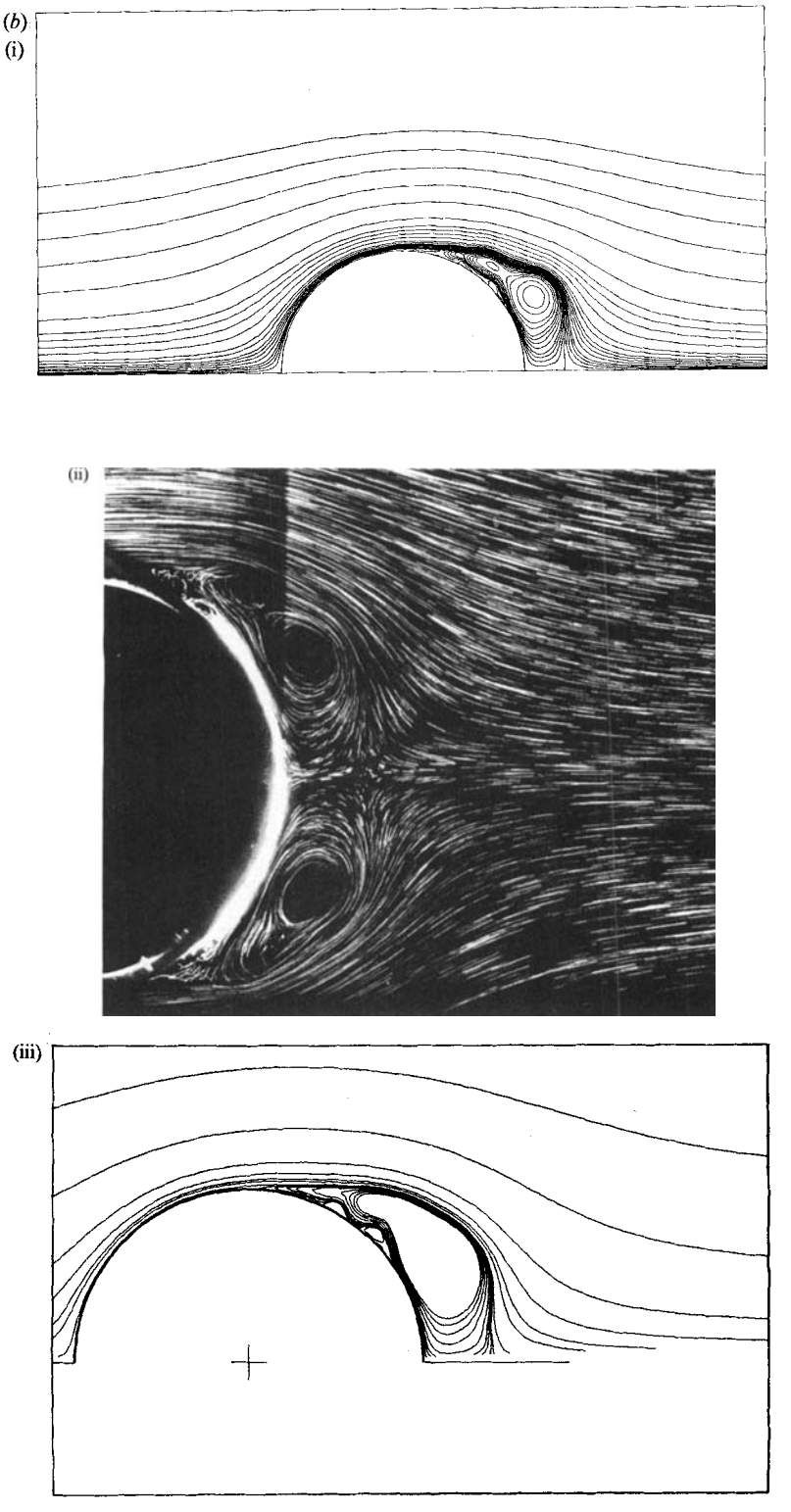


FIGURE 14(*b*). For caption see page 76.

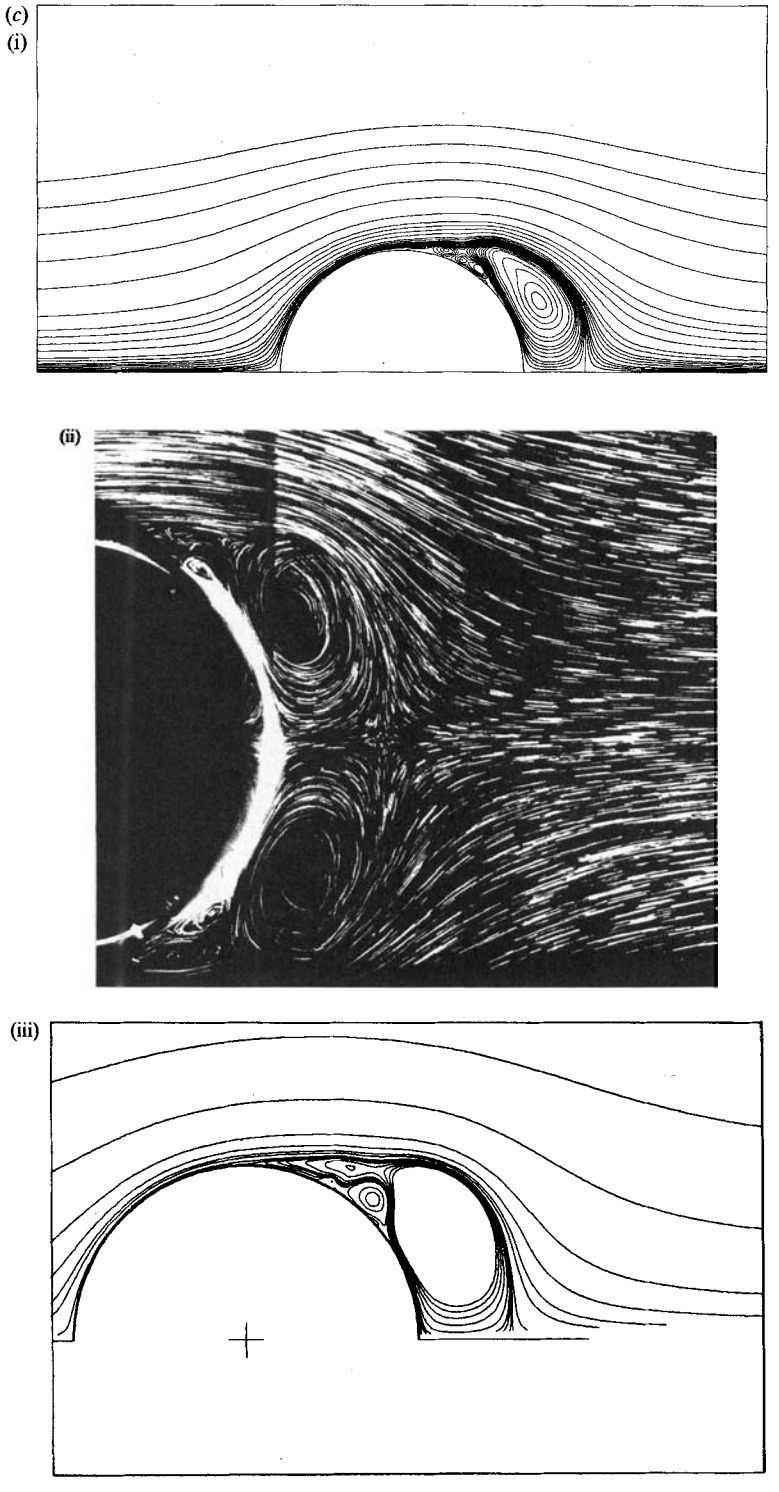


FIGURE 14(c). For caption see page 76.

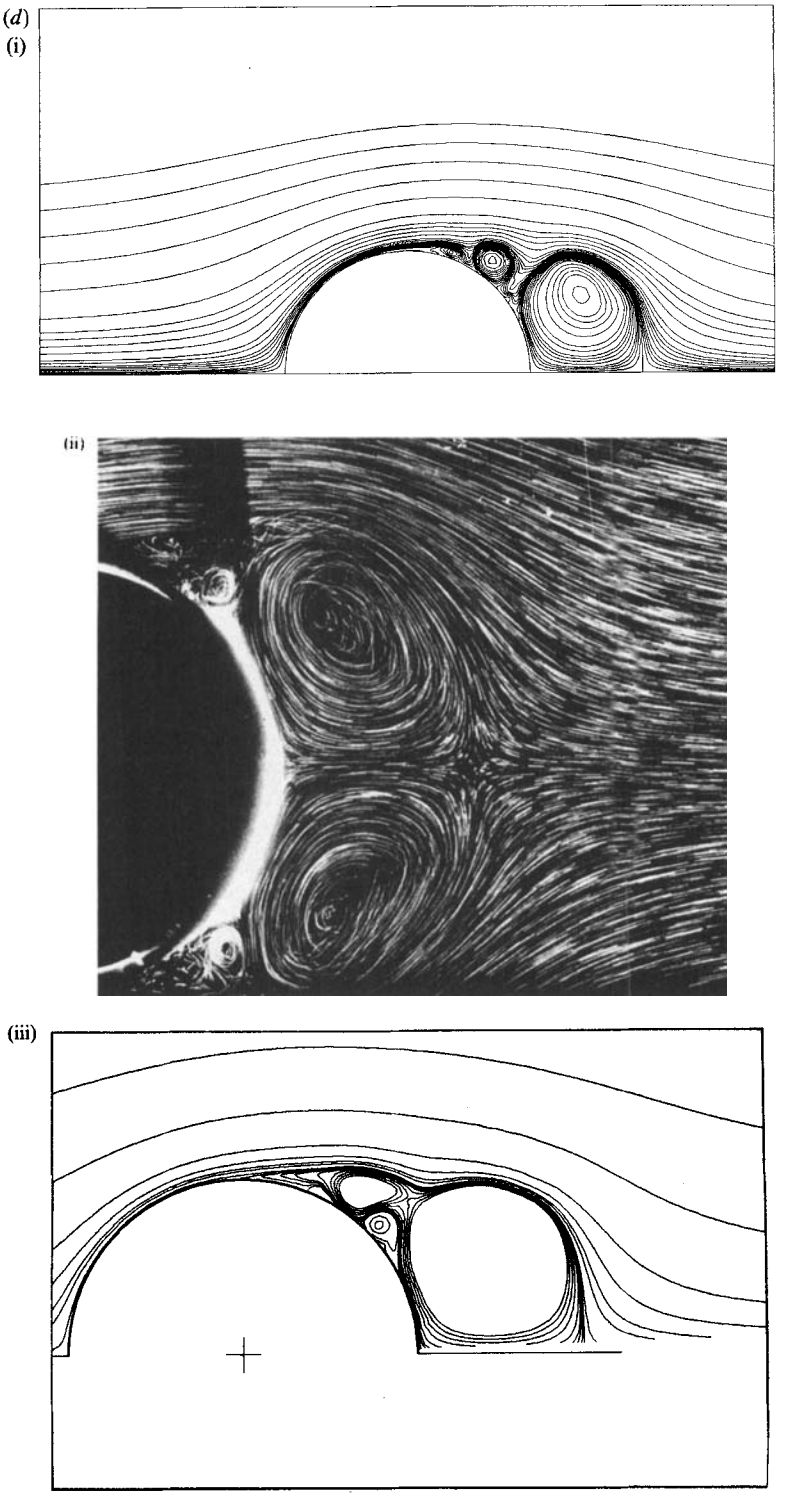


FIGURE 14. Comparison at $Re = 9500$ of the streamlines from the vortex method (i) with experimental visualizations (ii) and with streamlines from a finite-difference method (iii) (Ta Phuoc Loc & Bouard 1985). (*a*) $t = 1.6$; (*b*) $t = 2.8$; (*c*) $t = 3.2$; (*d*) $t = 4.0$.

these flows provided sufficient vortices are introduced. Long-time simulations (not presented here) indicate that the method always remains stable. It is generally considered that Eulerian simulations eventually become unstable without upwind differencing, introducing a source of error (Telionis 1981). This was not present in the accurate Eulerian methods mentioned above, which simulate flows of relatively short duration.

This work forms part of the research programme of the Marine Technology Directorate's Fluid Loading Programme, a programme of research jointly funded by SERC, the Department of Energy and the offshore industry. The authors would like to thank Professor H. T. Yang, for providing typographical corrections to the matched asymptotic expansion formulae in Bar-Lev & Yang (1975).

## REFERENCES

ANDERSON, C. R. 1986 A method of local corrections for computing the velocity field due to a distribution of vortex blobs. *J. Comp. Phys.* **62**, 111.

ANDERSON, C. R. & GREENGARD, C. 1985 On vortex methods. *SIAM J. Numer. Anal.* **22**, 413.

BAR-LEV, M. & YANG, H. T. 1975 Initial flow field over an impulsively started circular cylinder. *J. Fluid Mech.* **72**, 625.

BATCHELOR, G. K. 1981 *An Introduction to Fluid Dynamics*. Cambridge University Press.

BEALE, J. T. & MAJDA, A. 1981 Rates of convergence for viscous splitting of the Navier–Stokes equations. *Maths Comput.* **37**, 243.

BOUARD, R. & COUTANCEAU, M. 1980 The early stage of development of the wake behind an impulsively started cylinder for $40 < Re < 10^4$. *J. Fluid Mech.* **101**, 583.

CHEER, A. Y. 1983 Numerical study of incompressible slightly viscous flow past blunt bodies and airfoils. *SIAM J. Sci. Stat. Comp.* **4**, 685.

CHORIN, A. J. 1973 Numerical study of slightly viscous flows. *J. Fluid Mech.* **57**, 785.

CHORIN, A. J. 1978 Vortex sheet approximation of boundary layers. *J. Comp. Phys.* **27**, 428.

CHORIN, A. J. 1980 Vortex models and boundary layer instability. *SIAM J. Sci. Stat. Comp.* **1**, 1.

CHRISTIANSEN, J. P. 1973 Vortex methods for flow simulation. *J. Comp. Phys.* **13**, 363.

COLLINS, W. M. & DENNIS, S. C. R. 1973*a* The initial flow past an impulsively started circular cylinder. *Q. J. Mech. Appl. Maths* **26**, 53.

COLLINS, W. M. & DENNIS, S. C. R. 1973*b* Flow past an impulsively started circular cylinder. *J. Fluid Mech.* **60**, 105.

DAVIS, R. W. & MOORE, E. F. 1982 A numerical study of vortex shedding from rectangles. *J. Fluid Mech.* **116**, 475.

HOCKNEY, R. W. 1970 The potential calculation and some applications. *Methods Comp. Phys.* **9**, 135.

LEONARD, A. 1980 Vortex methods for flow simulation. *J. Comp. Phys.* **37**, 289.

QUARTEPELLE, L. & NAPOLITANO, M. 1983 Force and moment in incompressible flows. *AIAA J.* **21**, 911.

ROBERTS, S. 1985 Accuracy of the random vortex method for a problem with non-smooth initial conditions. *J. Comp. Phys.* **58**, 29.

SMITH, P. A. & STANSBY, P. K. 1987 Generalised discrete vortex method for cylinders without sharp edges. *AIAA J.* **25**, 199.

STANSBY, P. K. & DIXON, A. G. 1983 Simulation of flows round cylinders by a Lagrangian vortex scheme. *Appl. Ocean Res.* **5**, 167.

TA PHUOC LOC & BOUARD, R. 1985 Numerical solution of the early stage of the unsteady viscous flow around a circular cylinder: a comparison with experimental visualisation and measurements. *J. Fluid Mech.* **160**, 93.

TELIONIS, D. P. 1981 *Unsteady Viscous Flows*. Springer.

TRITTON, D. J. 1977 *Physical Fluid Dynamics*. Van Nostrand Reinhold.

WAX, N. 1954 *Selected Papers on Noise and Stochastic Processes*. Dover.